Ph.D. DISSERTATION

A Study on Underwater Acoustic Source Localization using Compressive Sensing-Based Approach

압축센싱 기반 접근법을 이용한 수중음향 소음원의 위치 추정 기법 연구

BY

Minseuk Park

FEBRUARY 2021

DEPARTMENT OF NAVAL ARCHITECTURE AND
OCEAN ENGINEERING
COLLEGE OF ENGINEERING
SEOUL NATIONAL UNIVERSITY

압축센싱 기반 접근법을 이용한 수중음향 소음원의 위치 추정 기법 연구

A Study on Underwater Acoustic Source Localization using Compressive Sensing-Based Approach

지도교수 성 우 제

이 논문을 공학박사 학위논문으로 제출함

2020년 12월

서울대학교 대학원

조선해양공학과

박 민 석

박민석의 공학박사 학위논문을 인준함

2020년 12월

위 원 장 : 김 태 완 (인)

부위원장 : 성 우 제 (인)

위 원 : 이 신 형 (인)

위 원 : 박 철 수 (인)

위 원 : 추 영 빈 (인)

Abstract

Three-dimensional acoustic localization is an essential process to analyze the underwater sound sources such as submarine, scatterer, marine cavitation. Traditional beamforming processors provide robust localization results, however, the results show a low-resolution result which only reveals one dominant source location. In order to obtain the high resolution localization results, compressive sensing(CS) based approaches have been used recently. CS technique is an effective way for acquiring, processing, reconstructing the sparse signal and has wide applicability to many research fields such as image processing, underwater acoustics and optimization problems. For localizing the underwater acoustic sources, CS-based approaches have been adopted in many research fields and have shown better localization performance compared to the traditional beamforming processors in terms of resolution. Despite the performance improvement in resolution, there are still problems that need to be resolved when using the CS-based method. First, the CS-based method does not appear to be robust compared with the traditional beamforming processors. CS-based method provides high-resolution results, however, it suffers from computational instability which hinders the stable reconstruction. Second, basis mismatch error hindrances estimating the exact source locations. Moreover, there is no basis mismatch estimation technique applicable to 3D source localization problem.

This dissertation points out the limitation of conventional CS-based localization method and introduces the advanced CS-based localization method which deals with 3D source localization problem. The “coherent multiple-frequency processing” is introduced to overcome the instability of solution induced by high correlation of spatial grids and “flexible searching-grid technique” is introduced to solve the basis mismatch problem which is developed for 3D source localization problem. The suggested tech-

niques provide more accurate localization results compared to traditional beamforming processors or conventional CS-based beamforming processors and the arguments are backed with actual experimental data which was conducted in a cavitation tunnel. Though underwater acoustic source localization problems are presented in this dissertation, the proposed technique can be extended to many research fields, such as radar detection, sonar detection, ultrasound imaging.

Keywords: Compressive Sensing, Beamforming, Cavitation, Localization, Block-sparsity, Sparse Bayesian Learning

Student number: 2015-21164

Contents

List of Figures

List of Tables

Phrases and their abbreviations

Abbreviation Phrase

TDOA, Time difference of arrivals

MFP, Matched field processing

CBF, Conventional beamforming

CS, Compressive sensing

BSCS, Block-sparse compressive sensing

SBL, Sparse Bayesian learning

OGSBI, Off gird sparse Bayesian inference

TVC, Tip vortex cavitation

Chapter 1

Introduction

Marine source localization, such as DOA estimation[1], source localization[2], sonar detection[3], is an essential process in underwater acoustics. Acoustic source localization results provide not only spatial information but also the characteristics of noise sources. For this reason, an accurate source localization processor is essentially required. TDOA(Time Differential of Arrival) methods[4] and beamforming processors[5] are popular strategies for localizing the acoustic sources. The TDOA method calculates the arrival time differences from sources to hydrophones which provides proper location of acoustic source. But this method is generally conducted in time-domain, it suffers from background noise and multi-path effect.[4, 6] Beamforming processors calculate the amplitudes and difference of phases for each hydrophones. This processor is generally conducted in frequency-domain. Thus, it is robust to background noise so that it has been widely applied to underwater acoustic source localization problems.[2] For the three-dimensional beamforming processor, the localization results are shown as an ambiguous surface. The ambiguity surface does not provide distinct source locations but provides an acoustic center.[7] The acoustic center indicates exact source location in the case that only one acoustic source exists in the search space. However, the acoustic center is not a convincing location of the acoustic source when there are many distributed sources.

In recent years, a series of studies on CS-based[8] localization have been developed in underwater acoustics.[9–14] For example, CS technique have been applied to DOA estimation problem and have shown that high-resolution DOAs can be presented compared to traditional beamforming processors.[1, 9] Recently, shallow water location mapping[11] and cavitation noise source localization results[15] have been presented using CS-based technique and have shown that CS technique is also applicable to the localization problem in 2-D and 3-D problem. These CS-based localization results have shown that sparse reconstruction is an effective way to extract the spatially sparse locations and has capability of high-resolution result compared to traditional beamforming processors. Despite the performance improvement in resolution, CS-based localization methods have problems which could disturb the exact localization result. First, exact reconstruction is sometimes problematic when the computational complexity is high. Especially, three-dimensional localization system has massive spatial bases so that stable source reconstruction is problematic.[16] Second, CS-based localization methods suffer from a basis mismatch issue. When the actual source positions are not located on the discretized searching grids($i.e.$, spatial bases), it is referred that there is a basis mismatch.[17] The basis mismatch is a very critical issue for the CS-based localization methods, which results in incorrect determination of the number and locations of the sources. One possible way to reduce the basis mismatch is to exploit the off grid techniques.[18, 19] However, the off grid techniques have been only developed for the 1D[20] and 2D[21] cases, the off grid technique which is applicable to 3D case has not been developed yet.

For these reasons, this dissertation presents advanced CS-based localization methods to resolve these problems. Two CS-based 3D source localization methods are suggested : “coherent multi-frequency processing” which reduces the computational instability (Chapter 3) and “flexible searching-grid method” which reduces the basis mismatch error (Chapter 4). These methods provide robust and accurate localization results compared to conventional CS-based approaches and the arguments are backed

with simulation and experimental results.

1.1 Issue 1 : Computational Stability

When we receive the acoustic source signal by using the hydrophone, the signal can be represented in the three representative domains : space, time and frequency. In the aspect of sparse reconstruction, the acoustic source signals are generally sparse since the number of searching grids are larger than the number of acoustic sources. Thus, the signal can be regarded as sparse in the space domain. If the acoustic source is stationary regardless of time varying, the signal is sparse in space domain and is clustered in time domain. This signal type is referred to be “joint-sparse” or “block-sparse”. The block-sparse CS is an effective signal reconstruction technique which enhances the reconstruction performance.The block-sparse CS provides better reconstruction properties than conventional CS technique when treating the block-sparse signal. For stationary acoustic sources, the BSCS technique[22] has been widely adopted to solve the MMVs problem and has shown that recovery performance can be significantly improved by using the BSCS.[23]

We further assumed that the source emits impulsive and wideband signal. Then, the signal will be sparse in space domain and will be clustered in frequency domain. This signal is also “block-sparse” in the spatial-spectral domain. Exploiting this block-sparse characteristic of the signal, we propose a broadband source localization method by using BSCS, which is referred to as “coherent multi-frequency processing”.

By promoting the block-sparsity in the spatial-frequency domain, the proposed localization approach provides the stable and accurate localization results compared to the conventional CS-based approaches. To validate the localization performance, this approach is demonstrated on experimental data from a transducer source experiment and a cavitation source experiment.

1.2 Issue 2 : Basis Mismatch

Conventional CS-based localization approaches are conducted in discrete spatial domain. In other words, the approaches employ finite discrete grid points to estimate the source location by using sparse signal feature. One issue for the conventional CS-based localization approaches is basis-mismatch, which occurs when the exact K support (the true source locations of searching grids) does not locate on the discretized grid point. This basis mismatch results in numerical error and hinders the accurate source localization. To prevent the basis mismatch error, the off grid techniques have been developed. The off grid techniques estimate the basis mismatch by usage of the atomic-norm minimization method[18] or the posterior maximization method[19]. Then, the estimated basis mismatch errors are compensated to the reconstruction signal.

Unlike CS-based localization methods conducted in 1D and 2D domains, the off grid technique applicable to 3D domain has not been developed yet. The difficulty occurs by that first-order linearization of the transfer function is hard to be achieved in the 3D domain. (Further discussion will be presented in Chapter 4)

In this dissertation, we firstly propose the basis-mismatch error estimation processor applicable to 3D source localization problem. To resolve the linearization issue, we introduce the "flexible searching-grid" technique. The position of flexible searching-grid is designed to be varied with each iteration and to be converged to true source position regardless of the linearization issue. By reducing the basis-mismatch error, the proposed off grid technique provides the accurate localization results compared to the conventional CS-based approaches.

1.3 Organization of the Dissertation

The remainder of this dissertation is organized as follows. In Chapter 2, CS algorithms used in this dissertation are briefly expressed. Chapter 3 introduces the "coherent multiple-frequency processing" and Chapter 4 introduces the "flexible searching

grid" technique. Chapter 5 concludes this dissertation with contributions of the research.

References

[1]A. Xenakia and P. Gerstoft, "Compressive beamforming", J. Acoust. Soc. Am. **136**, 260–271 (2014).

[2]C. Park, H. Seol, K. Kim, and W. Seong, "A study on propeller noise source localization in a cavitation tunnel", Ocean Eng. **36**, 754–762 (2009).

[3]M. A. Ainslie, *Principles of sonar performance modeling* (Springer, New York), pp. 1–122.

[4]N. A. Chang and D. R. Dowling, "Ray-based acoustic localization of cavitation in a highly reverberant environment", J. Acoust. Soc. Am. **125**, 3088–3100 (2009).

[5]A. Tolstoy, *Matched field processing for underwater acoustics* (World Scientific Publishing, Singapore, 1993) Chap. 4, pp. 91–180.

[6]N. A. Chang and S. L. Ceccio, "The acoustic emissions of cavitation bubbles in stretched vortices", J. Acoust. Soc. Am. **130**, 3209–3219 (2011).

[7]D. Kim, W. Seong, Y. Choo, and J. Lee, "Localization of incipient tip vortex cavitation using ray based matched field inversion method", J. Sound Vib. **354**, 34–46 (2015).

[8]D. L. Donoho, "Compressed sensing", IEEE Trans. Inf. Theory **52**, 1289–1306 (2006).

[9]D. Malioutov, M. Cetin, and A. Willsky, "A sparse signal reconstruction perspective for source localization with sensor arrays", IEEE Trans. Signal Process. **53**, 3010–3022 (2005).

[10]C. Yardim, P. Gerstoft, W. S. Hodgkiss, and J. Traer, "Compressive geoacoustic inversion using ambient noise", J. Acoust. Soc. Am. **135**, 1245–1255 (2014).

[11]P. A. Forero and P. A. Baxley, "Shallow-water sparsity-cognizant source-location mapping", J. Acoust. Soc. Am. **135**, 3483–3501 (2014).

[12]G. Chardon, L. Daudet, A. Peillot, F. Ollivier, N. Bertin, and R. Gribonval, "Near-field acoustic holography using sparse regularization and compressive sampling principles", J. Acoust. Soc. Am. **132**, 1521–1534 (2012).

[13]E. Fernandez-Grande, A. Xenaki, and P. Gerstoft, "A sparse equivalent source method for near-field acoustic holography", J. Acoust. Soc. Am. **141**, 532–542 (2017).

[14]N. Wagner, Y. C. Eldar, and Z. Friedman, "Compressed beamforming in ultrasound imaging", IEEE Trans. Signal Process. **60**, 4643–4657 (2012).

[15]Y. Choo and W. Seong, "Compressive spherical beamforming for localization of incipient tip vortex cavitation", J. Acoust. Soc. Am. **140**, 4085–4090 (2016).

[16]M. Park, Y. Park, K. Lee, and W. Seong, "Incipient tip vortex cavitation localization using block-sparse compressive sensing", J. Acoust. Soc. Am. **147**, 3454–3464 (2016).

[17]Y. Chi, L. L. Scharf, A. Pezeshki, and A. R. Calderbank, "Sensitivity to basis mismatch in compressed sensing", IEEE Trans. Signal Process. **59**, 2182–2195 (2011).

[18]E. J. Candes and C. Fernandez-Granda, "Towards a mathematical theory of super-resolution", Comm. Pure Appl. Math. **67**, 906–956 (2013).

[19]Z. Yang, L. Xie, and C. Zhang, "Off-grid direction of arrival estimation using sparse bayesian inference", IEEE Trans. Signal Process. **61**, 38–43 (2013).

[20]A. Xenaki and P. Gerstoft, "Grid-free compressive beamforming", J. Acoust. Soc. Am. **137**, 1923–1935 (2015).

[21]Y. Yang, Z. Chu, Z. Xu, and G. Ping, "Two-dimensional grid-free compressive beamforming", J. Acoust. Soc. Am. **142**, 618–629 (2017).

[22]Y. C. Eldar, P. Kuppinger, and H. Bolcskei, "Block-sparse signals : uncertainty relations and efficient recovery", IEEE Trans. Signal Process. **58**, 3042–3054 (2010).

[23]P. Gerstoft, A. Xenaki, and C. F. Mecklenbräuker, "Multiple and single snapshot compressive beamforming", J. Acoust. Soc. Am. **138**, 2003–2014 (2015).

Chapter 2

CS techniques for three-dimensional source localization

In this dissertation, advanced CS-based approaches are developed exploiting the conventional CS techniques for estimating the precise 3D source locations. In this chapter, several conventional CS algorithms are briefly explained to improve the reader's comprehension. The CS[1] and BSCS[2] algorithms are described in Section 2.1 and 2.2. These algorithms are the basic background of Chapter 3. The SBL[3] and OGSBI[4] algorithms are described in Section 2.3 and 2.4. These algorithms are the basic background of Chapter 4.

2.1 Compressive Sensing (CS)

CS[1] is a signal reconstruction technique applicable to sufficiently sparse signals with less measurement data. Many underwater acoustic source signals have a much lower level of information than their dimension. For example, the number of underwater acoustic sources are generally smaller than the number of searching grids.

Let $\mathbf{x} \in \mathbb{C}^N$ be an unknown vector representing the complex amplitude of sources which located in certain grid points $\mathbf{y} \in \mathbb{C}^M$ be a measurement vector from sources to receivers. Then, $\mathbf{x}$ and $\mathbf{y}$ are related by a linear set of equations which can be described

as below,

$$\mathbf{y} = \mathbf{A}\mathbf{x} + \mathbf{n}, \tag{2.1}$$

where $\mathbf{A}$ is a sensing matrix and $\mathbf{n}$ is a noise vector. Generally, $\mathbf{N}$ is much larger than $\mathbf{M}(i.e., \mathbf{N} \gg \mathbf{M})$, this linear system is underdetermined. However, if $\mathbf{K}$ non-zero components of $\mathbf{x}$ are sufficiently small($i.e.$, $\mathbf{x}$ is sparse), then this linear system can be solved by using the CS principle.

The CS principle assumes that signal to be reconstructed is sparse in some domain. In other words, the signal should have relatively few non-zero components. Thus, we can estimate the actual solution by seeking the most sparse solution within the numerous solutions. By using the CS technique, the original $\mathbf{K}$-sparse vector $\mathbf{x}$ can be reconstructed by the following solution.

$$\min_{\mathbf{x}\in\mathbb{C}^N} \ \|\mathbf{x}\|_0 \text{ subject to } \ \|\mathbf{y} - \mathbf{A}\mathbf{x}\|_2 \leq \epsilon, \tag{2.2}$$

where $\|\mathbf{x}\|_0$ and ϵ denote the number of non-zero components of $\mathbf{x}$ and noise error constraint. Note that Eq. (2.2) is an ill-posed problem since the calculation of l_0-norm is a trivial problem. Thus, Eq. (2.2) should be replaced for reducing the computational burden as follow.

$$\min_{\mathbf{x}\in\mathbb{C}^N} \ \|\mathbf{x}\|_1 \text{ subject to } \ \|\mathbf{y} - \mathbf{A}\mathbf{x}\|_2 \leq \epsilon, \tag{2.3}$$

(2.2) is referred as the l_1-norm minimization method. It has been proven that (2.2) and (2.3) equally work when x is sufficiently sparse. Then, by solving the Eq. (2.3), we can obtain the reconstructed signals from a few measurement data.

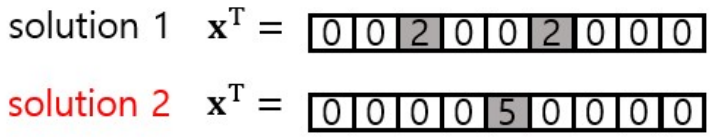

Figure 2.1: (a) K=2 sparse solution (b) K=1 sparse solution

2.2 Block-Sparse Compressive Sensing (BSCS)

To reconstruct the origin signal by using the CS-based approach, it is essentially required that the signal should be represneted as a sparse signal. In many practical applications, however, finding the sparse representation is problematic. For example, if non-zero components of the signal are clustered in certain positions, the clusters are sparse rather than non-zero components are sparse. This clustered signal is called block-sparse.

In terms of raw CS principle, block-sparse signal is not a sparse signal. However, by treating the clusters as blocks, BSCS enable this block-sparse signal to be reconstructed in terms of sparse recovery.

Let $\mathbf{x} \in \mathbb{C}^{NL}$ be a block-sparse signal vector. Then, the signal vector can be described as block structure.

$$\begin{aligned}\mathbf{x} &= [\mathbf{x}_1^{\text{block}}; \cdots ; \mathbf{x}_N^{\text{block}}] \\ &= [\underbrace{x_1^{(1)}, \cdots , \tilde{x}_1^{(L)}}_{\tilde{\mathbf{x}}_1^{\text{block}}}, \cdots , \underbrace{x_N^{(1)}, \cdots , x_N^{(L)}}_{\mathbf{x}_N^{\text{block}}}]^{\mathsf{T}},\end{aligned} \tag{2.4}$$

Then, the sparsity level of this system is determined by the number of non-zero blocks rather than the number of non-zero components. In other words, reconstruction procedure is processed to minimize the number of non-zero blocks.

$$\min_{\mathbf{x}\in\mathbb{C}^{NL}} \sum_{n=1}^{N} \mathbf{I}(\|\mathbf{x}_n^{\text{block}}\|_2 > 0) \;\text{ subject to }\; \|\mathbf{y}-\mathbf{A}\mathbf{x}\|_2 \leq \epsilon, \tag{2.5}$$

Eq.(2.6) represent the principle solution of the block-sparse signal reconstruction. However, Eq.(2.6) is also an ill-posed problem. Instead, Eq. (2.2) can be replaced for reducing the computational burden as follows.

$$\min_{\mathbf{x}\in\mathbb{C}^{NL}} \sum_{n=1}^{N} \|\mathbf{x}_n^{\text{block}}\|_2 \;\text{ subject to }\; \|\mathbf{y}-\mathbf{A}\mathbf{x}\|_2 \leq \epsilon, \tag{2.6}$$

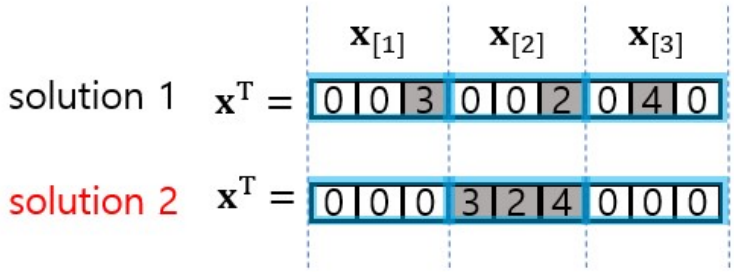

Figure 2.2: (a) K=3 block-sparse solution (b) K=1 block-sparse solution

2.3 Sparse Bayesian learning (SBL)

Sparse Bayesian Learning(SBL) is a kind of compressive sensing approach which uses a probabilistic model. In the SBL framework, the sparse signal vector $\mathbf{x}$ is treated as random variables and is reconstructed by maximizing the posterior. The approach seems to be similar to the MAP processor, however, there are two distinct features compared to MAP processor.

First, SBL has a parameterized prior. The parameterized prior can be described as below.

$$p(\mathbf{x}|\boldsymbol{\gamma}) = \prod_{i=1}^{N} p(x_i|\gamma_i) \tag{2.7}$$

where,

$$p(x_i;\gamma_i) = \frac{1}{\sqrt{2\pi\gamma^2}} \exp(-\frac{x_i^2}{2\gamma_i}) \tag{2.8}$$

$\boldsymbol{\gamma}$ is a hyper-parameter vector which controls the sparsity level. Theparameterized prior allows the posterior probability mass to concentrate at very large values of some of these $\boldsymbol{\gamma}$ variables. Thus, the reconstructed $\mathbf{x}$ could be sparse. And, as seen in 2.7 and 2.8, these hyperpriors are independent and (usually zero mean) multivariate Gaussian distribution.

Second, the SBL uses a Gaussian likelihood model.

$$p(\mathbf{y}|\mathbf{x},\sigma^2) = \frac{1}{(2\pi\sigma^2)^{\frac{N}{2}}} \exp(-\frac{1}{2\sigma^2}||\mathbf{y}-\mathbf{A}\mathbf{x}||_2^2) \tag{2.9}$$

According to 2.9, obtaining maximum likelihood estimates for under this condition is equivalent to minimizing the $l2$-norm solution to 2.1 To avoid "over-fitting" issue in MAP processor, SBL impose a "comprexity" penalty term($i.e.$, regularisation) to the prior distribution defined by "hyperpriors".

By using these features, SBL derives a fully probabilistic posterior model.

$$p(\mathbf{x}|\mathbf{y},\boldsymbol{\gamma},\sigma^2) = \frac{likelihood \times prior}{normalising\ factor} = \frac{p(\mathbf{y}|\mathbf{x},\sigma^2) \times p(\mathbf{x}|\boldsymbol{\gamma})}{p(\mathbf{y}|\boldsymbol{\gamma},\sigma^2)} \tag{2.10}$$

In 2.10, unknown parameters are $\boldsymbol{\gamma}, \sigma^2$. Thus, we can obtain the sparse solution $\mathbf{x}$ by estimating the proper parameters $\boldsymbol{\gamma}, \sigma^2$ which maximize the posterior $p(\mathbf{x}|\mathbf{y},\boldsymbol{\gamma},\sigma^2)$.

2.4 Off-Grid Sparse Bayesian Inference (OGSBI)

For reducing the basis mismatch, off grid sparse Bayesian inference(OGSBI) approach had been developed. OGSBI, based on SBL theory, estimates the basis mismatch by maximizing the posterior of the system below.

$$\mathbf{y} - (\mathbf{A} + \mathbf{D}\boldsymbol{\Delta})\mathbf{x} \tag{2.11}$$

$\mathbf{D}$ is a linearization matrix and $\boldsymbol{\Delta}$ is a basis mismatch vector. By maximizing the posterior, we can directly obtain the basis mismatch factors.

By exploiting the Eq.(2.11), the sparse Bayesian formulation can be derived as follow

1) sparse signal model to maximize the posterior The posterior distribution can be described as below.

$$p(\mathbf{y},\mathbf{x};\boldsymbol{\gamma},\sigma^2,\boldsymbol{\Delta}) = p(\mathbf{y}|\mathbf{x};\sigma^2,\boldsymbol{\Delta})p(\mathbf{x}|\boldsymbol{\gamma}) \tag{2.12}$$

where, prior $p(\mathbf{x}|\boldsymbol{\gamma})$ is multi-variate guassian distribution,

$$p(\mathbf{x}|\boldsymbol{\gamma}) = \mathcal{CN}(\mathbf{x}|0,\boldsymbol{\gamma}) \tag{2.13}$$

and liklihood is,

$$p(\mathbf{y}|\mathbf{x};\sigma^2,\boldsymbol{\Delta}) = (\pi\sigma^2)^{-N}\exp(-\frac{1}{\sigma^2}||\mathbf{y}-(\mathbf{A}+\mathbf{D}\boldsymbol{\Delta})\mathbf{x}||_2^2) \tag{2.14}$$

According to Bayes' rule, posterior can be expressed as follow

$$p(\mathbf{y},\mathbf{x};\boldsymbol{\gamma},\sigma^2,\boldsymbol{\Delta}) = p(\mathbf{y}|\mathbf{x};\sigma^2,\boldsymbol{\Delta})p(\mathbf{x};\boldsymbol{\gamma}) \tag{2.15}$$

2) parameter estimation

The parameter estimation can be conducted by using the EM approach which consists of iterative E-steps and M-steps. (E-steps for estimating $\mathbf{x}$ and M-step for estimating the parameters $\boldsymbol{\gamma}, \sigma^2, \boldsymbol{\Delta}$)

(E-step : estimate $\boldsymbol{\Sigma}$ and $\mathbf{x}$)

$$\boldsymbol{\mu}_x = \boldsymbol{\Gamma}(\mathbf{A}+\mathbf{D}\boldsymbol{\Delta})^H\boldsymbol{\Sigma}_y^{-1}\mathbf{y} \tag{2.16}$$

where,

$$\begin{aligned}\boldsymbol{\Sigma} &= \boldsymbol{\Gamma} - \boldsymbol{\Gamma}(\mathbf{A}+\mathbf{D}\boldsymbol{\Delta})^H\boldsymbol{\Sigma}_y^{-1}(\mathbf{A}+\mathbf{D}\boldsymbol{\Delta})\boldsymbol{\Gamma} \\ \boldsymbol{\Sigma}_t &\triangleq \sigma^2\mathbf{I}_N + (\mathbf{A}+\mathbf{D}\boldsymbol{\Delta})\boldsymbol{\Gamma}(\mathbf{A}+\mathbf{D}\boldsymbol{\Delta})^H\end{aligned} \tag{2.17}$$

(M-step : estimate $\sigma^2, \boldsymbol{\gamma}, \boldsymbol{\Delta}$)

For estimating the $\boldsymbol{\gamma}$, maximize $E_{\mathbf{y},\mathbf{x};\boldsymbol{\gamma},\sigma^2,\boldsymbol{\Delta}}[\log p(\mathbf{x}|\boldsymbol{\gamma})]$;

$$\boldsymbol{\gamma} = ||x_i||_2^2 + \boldsymbol{\Sigma}_{ii}, for\ i = 1, ..., N \tag{2.18}$$

For estimating the σ^2, maximize $E_{\mathbf{y},\mathbf{x};\gamma,\sigma^2,\Delta}[\log p(\mathbf{y}|\mathbf{x};\sigma^2,\boldsymbol{\Delta})]$

$$\sigma^2 = \frac{1}{N}\big[||\mathbf{y} - (\mathbf{A} + \mathbf{D}\boldsymbol{\Delta})\mathbf{x}||_2^2 + Tr((\mathbf{A} + \mathbf{D}\boldsymbol{\Delta})^H(\mathbf{A} + \mathbf{D}\boldsymbol{\Delta})\boldsymbol{\Sigma})\big] \tag{2.19}$$

For estimating $\boldsymbol{\Delta}$, maximizing the $E_{\mathbf{y},\mathbf{x};\gamma,\sigma^2,\boldsymbol{\Delta}}[\log p(\mathbf{y}|\mathbf{x};\sigma^2,\boldsymbol{\Delta})]$ is equivalent to minimize,

$$\begin{aligned} & E\Big\{||\mathbf{y} - (\mathbf{A} + \mathbf{D}\boldsymbol{\Delta})\mathbf{x}||_2^2\Big\} \\ =& ||\mathbf{y} - (\mathbf{A} + \mathbf{D}\boldsymbol{\Delta})\boldsymbol{\mu}_x||_2^2 + Tr\Big\{(\mathbf{A} + \mathbf{D}\boldsymbol{\Delta})\boldsymbol{\Sigma}(\mathbf{A} + \mathbf{D}\boldsymbol{\Delta})^H\Big\} \\ =& \boldsymbol{\Delta}\mathbf{Q}\boldsymbol{\Delta} + 2\mathbf{R}\boldsymbol{\Delta} + \mathbf{C} \end{aligned} \tag{2.20}$$

Thus, the basis mismatch $\boldsymbol{\Delta}$ can be estimated by minimizing the following equation.

$$\arg\min_{\boldsymbol{\Delta}} \big\{\boldsymbol{\Delta}\mathbf{Q}\Delta + 2R\boldsymbol{\Delta}\big\} \tag{2.21}$$

$$\boldsymbol{\Delta} = \mathbf{Q}^{-1}\mathbf{R} \tag{2.22}$$

where,

$$\begin{aligned} \mathbf{Q} &= \mathrm{Re}[\mathbf{D}^H\mathbf{D} \odot (\boldsymbol{\mu}_x^H\boldsymbol{\mu}_x + \boldsymbol{\Sigma})] \\ \mathbf{R} &= \mathrm{Re}[diag(\boldsymbol{\mu}_x)\mathbf{D}^H\mathbf{y} - \mathbf{A}\mu_x] - \mathrm{Re}[diag(\mathbf{D}^H\mathbf{A}\boldsymbol{\Sigma})] \end{aligned} \tag{2.23}$$

References

[1]D. L. Donoho, “Compressed sensing”, IEEE Trans. Inf. Theory **52**, 1289–1306 (2006).

[2]Y. C. Eldar, P. Kuppinger, and H. Bolcskei, “Block-sparse signals : uncertainty relations and efficient recovery”, IEEE Trans. Signal Process. **58**, 3042–3054 (2010).

[3]M. E. Tipping, “Sparse bayesian learning and the relevance vector machine”, J. Mach. Learn. Res. **1**, 211–244 (2001).

[4]Z. Yang, L. Xie, and C. Zhang, “Off-grid direction of arrival estimation using sparse bayesian inference”, IEEE Trans. Signal Process. **61**, 38–43 (2013).

Chapter 3

3D CS-based source localization method using multiple-frequency components

3.1 Introduction

Marine propeller cavitation is a dominant noise source phenomenon; [1] thus, it is essential to infer its inception and, possibly, its precise location. Cavitation is of a broadband nature, and previous studies to detect and localize the source of cavitation noise based on the matched-field processing (MFP) method [2] or compressive sensing (CS) method [3] adopted frequency-domain broadband approaches, producing reasonable localization results. The CS-based method [4] showed better localization performance than that of the MFP-based methods. [5–7] However, the CS-based method is not robust to noise compared with the MFP-based method. The aim of this study is to provide a propeller cavitation localization method based on CS that takes advantage of the robustness of the broadband approach to noise and the high-resolution capability of the CS-based method. For this purpose, the block-sparse CS [8–11] technique is adopted, which enables the joint retrieval of multi-frequency components.

Microbubbles incepted by a propeller tip vortex line radiate a short impulse signal during the processes of growth, split, and collapse, which is called tip vortex cavitation

(TVC). [1] When the bubbles grow large enough, vortex cavitation can be detected and localized by optical observation. However, optical observation is unavailable when optical access is not allowed or when bubbles are too small to be optically observed. Generally, in the incipient stage of TVC, incepted bubbles are small and invisible to the bare eye; thus, the optical approach is not an appropriate method. More practically, acoustical techniques, implemented either in the time domain [12, 13] or frequency domain, [4–7, 14, 15] can be used to detect and localize the cavitation noise source.

In the time domain, the time difference of arrival (TDOA)-based method is a popular strategy for source localization. The TDOA-based method achieves source localization without computational complexity. However, an accurate estimate of the arrival time is difficult in the presence of the multi-path effect. Generally, in the cavitation tunnel test, the received signal is distorted owing to multi-reflection and noisy environments. The separation of a multi-path signal is sometimes problematic when the received signal waveform is distorted. To localize the vortex cavitation, Chang and Dowling [12] used the TDOA-based method and presented the acoustical localization results. However, they suffered from the effects of reverberation, and additional signal processing had to be used [12, 13] to obtain the direct-path signal.

One possible way to mitigate the multi-path effect is to implement source localization in the frequency domain. When the waveform is distorted owing to the multi-path effect, frequency-domain measurement data can be alternatively utilized for source localization. In the case of TVC localization, the MFP-based method using single-frequency measurement data showed that accurate localization can be achieved despite the presence of the multi-path effect. [6] However, single-frequency measurement data still include a frequency interference pattern, reverberation, and background noise, all of which hinder accurate localization. Moreover, the single-frequency approach may not be effective under very low signal-to-ratio (SNR) conditions. These hindrances can be alleviated by using multi-frequency measurement data. [5–7] Because the received signal at a single frequency includes frequency-dependent infor-

mation, such as ambiguity surface patterns [2] or environmental characteristics, combining the frequency-dependent information leads to the minimization of unwanted information. There are a number of different ways to combine frequency-dependent information across frequencies, which can be categorized based on the coherence of the processing method. Incoherent multiple-frequency processing considers each aspect of frequency-dependent information independently of each other. Thus, the information for each frequency is processed individually and combined by direct averaging across frequencies. In contrast, coherent multiple-frequency processing considers each frequency-dependent piece of information cohesively.

The MFP-based method simulates a replica (modeled pressure field induced by a potential noise source) and compares the replica against the measured pressure field of a single frequency at a certain location. This process is performed over multiple frequencies of interest. Then, by exploiting the incoherent multiple-frequency processing, the similarity values are mathematically averaged over frequencies, and the estimation of potential noise source is reached. In the case of TVC noise source localization, Kim *et al.* [6] and Park *et al.* [7] utilized incoherent broadband MFP and showed successful localization results. Because TVC transmits broadband noise, the similarities between the replica and measured pressure field can be compared over multiple frequencies of interest. Despite the fact that each ambiguity surface at a single frequency includes frequency-dependent patterns and sidepeaks that hinder accurate localization, the averaged ambiguity surface effectively mitigates these hindrances. As a result, accurate source localizations were achieved using incoherent broadband MFP. [6, 7]

CS is a signal reconstruction technique [3] applicable to sufficiently sparse signals with less measurement data and has shown that it can be applied to the underlying acoustic models which have sparse representations in the basis, such as beamforming [16–18], geo-acoustic inversion [19], near-field acoustic holography [20–22] and underwater source localization [23]. Particularly, Xenaki *et al.* [17] utilized CS for DOA reconstruction to overcome the resolution limit of conventional beamforming

and showed that the received plane wave signals can be distinguished at high resolution.

Motivated by the CS-based beamforming method, [16, 17] Choo and Seong [4] extended the CS technique to the 3d-spherical beamforming problem using incoherent multiple-frequency processing. Because TVC noise sources can be modeled as few monopole-type broadband sources, [1, 6, 14] the received signals were approximated as the superposition of the spherical waves induced by potential noise sources. Then, to estimate the locations of the potential noise sources, a sparse reconstruction framework was proposed, assuming that the numerous potential sources are evenly distributed near the propeller region, and sparse reconstruction was performed for all potential sources. Exploiting incoherent multiple-frequency processing, the reconstruction process was conducted at each frequency, and the reconstructed potential sources were averaged across frequencies. In this manner, sparse components were shown to be evident in the averaged solution, which indicates the real source positions.

The CS-based method showed enhanced performance with respect to resolution, compared with the MFP-based method. Furthermore, the sparse reconstruction framework offers the additional advantage of not requiring the number of potential noise sources used for localization. When using the MFP-based method, the accuracy of localization is reliant on selecting how many potential noise sources should be used. [14] On the contrary, the CS-based method looks for the sparsest solution; thus, it is not necessary to consider how many potential sources there should be.

Despite the performance improvement in resolution, there are still problems that need to be resolved using the CS-based method. First, the CS-based method [4] does not appear to be robust to noise compared with the MFP-based method [6], requiring higher SNR for stable reconstruction. However, the time duration of the acoustic signals from cavitation was short, approximately 15 ms long, such that sufficient SNR could not be obtained from a cavitation event. Thus, the CS-based method can be applied only to the long-time-sampled data from several cavitation events. Second,

the CS-based method shows high-resolution localization result but only reveals one dominant source location. In other words, the CS-based method has no capacity to distinguish separate noise sources.

To overcome these shortcomings, we propose an incipient TVC localization method which consider the multiple frequency components jointly. The method assumes that if the preassumed positions (grids) of the potential sources coincide with the true source positions, only the multiple frequency components associated with the corresponding positions would have non-zero elements. Thus, it can be naturally inferred that these multi-frequency components share a spatially common sparse representation and are spectrally grouped together. Exploiting the common sparsity profile assumption, we provide a signal model that can process the multiple frequency components simultaneously and a reconstruction scheme to promote the common sparsity profile. Here, we refer to this joint multiple frequency handling as 'coherent multiple-frequency processing'. The coherent multiple-frequency processing can provide enhanced localization performance since it finds common sparse representations across different frequency ranges.

To promote the common sparsity profile, we utilize block-sparse CS technique [8] for the reconstruction scheme. If non-zero entries of solution occur only in several partitioned blocks ($i.e.$, the solution has sparse non-zero blocks), such signals are termed as block-sparse. And block-sparse CS technique provides better reconstruction properties than conventional CS technique when treating the block-sparse signal. [8] It has been shown that recovery performance can be significantly improved using block-sparse CS in the acoustic signal processing problems. For example, in MMV(multiple measurement vector) problem non-zero elements of every column are temporally correlated under the stationary source assumption. Hence, the solution has a small number of nonzero rows ($i.e.$, the solution is row block-sparse), so that localization performance can be enhanced by promoting spatio-temporal common sparsity. [10, 24–26] Another interesting application of block-sparse CS is sparse regularization ap-

proach. [27] In practical applications, many acoustic problems are not sparse but clustered in predefined basis and there is no prior knowledge of how block partitions lie in the solution. In this case, sparse regularization approach can be a useful tool which promotes the block-sparsity of the solution, and reconstruction performance can be enhanced compared to conventional CS approach. [28–30] Recently, a sparse Bayesian learning (SBL) framework [31] has been applied to the joint sparse problems. The SBL framework provides a probabilistic description between the sparse signal and given measured data, and can be extendedly applied to the block-sparse problem. In many applications (e.g., MMV [32, 33] and clustered sparse signal [34] problems), the SBL framework have been effectively used to reconstruct the block-sparse signals by enforcing a common sparsity profile. In this paper, block-sparse CS technique was applied to enforce a common sparsity profile of broadband sources. Because the multiple frequency components associated with the corresponding positions have non-zero elements, while all others have zero elements, non-zero components occur only in clusters ($i.e.$, this signal is block-sparse) and can be reconstructed using block-sparse CS. The reconstruction scheme promotes the common sparsity profile, and thus better localization performance can be achieved compared to the conventional CS approach.

One contribution of our study is the use of coherent multiple-frequency processing, which provides a simultaneous and accurate reconstruction scheme for localizing the broadband sources. For each frequency, complex amplitudes of a broadband source are represented by different dictionaries but share the common spatial grid. To promote this spatially common sparsity profile, we provide a block-diagonal matrix system that makes all of the multiple frequency components to be vectorized and the spatially joint components to be partitioned as a block. Then, we reconstruct complex amplitudes of multi-frequencies simultaneously exploiting block-sparse CS. Adapting this joint sparse constraint to the reconstruction process, coherent multiple-frequency processing achieves improved accuracy compared with incoherent multiple-frequency processing.

Another contribution is that the proposed method provides high-resolution capability to distinguish separate sources in proximity. Given closely located sources, a low-resolution model ($i.e.$, MFP [6] and incoherent multiple-frequency processing with CS [4]) localizes one dominant source around the true sources but cannot distinguish each source separately. However, the present model achieves high-resolution ability and estimates closely located TVC noise sources at locations identified visually, even with short time length signal.

In Section II, we describe coherent multiple-frequency processing using block-sparse CS model to localize the TVC noise source. Section III provides some experimental results to show the performance of the proposed approach, and the performance is compared against that of the conventional CS approach. Finally, Section IV provides the conclusion and contributions of the study.

3.2 Block-sparse Compressive Sensing for Incipient Tip Vortex Cavitation Localization

3.2.1 System framework for incipient tip vortex cavitation localization

Incipient TVC is cavitation observed in the vicinity of the propeller tips, more specifically, at the top center of the propeller. The noise source by TVC transmits a monopole-type spherical waveform in all directions and has a broadband frequency spectrum. [12, 13, 35, 36] In the cavitation tunnel, the noise measured at the hydrophones contain multiple paths components, including the direct path and other paths reflected by tunnel walls. [6] In the experiment, the noise source signal that corresponds to the direct path is dominant over the others. [6] Considering a single frequency f monopole source transmission, the received signal through the direct path at the mth hydrophone $y_m^{(f)}$ can be derived as

$$y_m^{(f)} = \frac{e^{-j(2\pi f/c)r_m}}{4\pi r_m} x^{(f)} + n_m^{(f)}, \tag{3.1}$$

where $y_m^{(f)}$ is the measured sound pressure, c is the water sound speed (here, we use 1502 m/s), r_m is the distance from the cavitation noise source to the mth hydrophone, $x^{(f)}$ is a complex amplitude which has magnitude and initial phase of the cavitation noise, and $n_m^{(f)}$ is the error that involves electric noise, experimental error, or mismatch between actual phenomena and modeling.

In the localization problem, the search space is discretized by potential noise source locations, and the objective is to find the actual locations of the (usually few) noise sources among the assumed potential locations. Let $\mathbf{x}^{(f)} \in \mathbb{C}^N$ be an (sparse) unknown vector we aim to reconstruct, where N is the number of discretized potential locations of noise sources.

The measurement data at the mth hydrophone Eq. (3.1), which is the superposition of spherical waves from N potential sources, can be expressed using potential noise sources $\mathbf{x}^{(f)}$,

$$y_m^{(f)} = \sum_{n=1}^{N} \frac{e^{-j(2\pi f/c)r_{m,n}}}{4\pi r_{m,n}} x_n^{(f)} + n_m^{(f)}, \tag{3.2}$$

where $r_{m,n}$ is the distance from the mth hydrophone to the nth potential noise source, and the unknown vector $\mathbf{x}^{(f)}$ is composed of N complex amplitudes. Note that a fine resolution localization performance is desired; thus, $M \ll N$.

Then, the relationship between M hydrophones and N potential noise sources can be expressed as below

$$\mathbf{y}^{(f)} = \mathbf{A}^{(f)}\mathbf{x}^{(f)} + \mathbf{n}^{(f)}, \tag{3.3}$$

where $\mathbf{y}^{(f)}$ is the measurement vector at M hydrophones $\mathbf{y}^{(f)} \in \mathbb{C}^M$, and the (m, n)th

entry of the matrix $\mathbf{A}^{(f)} \in \mathbb{C}^{M\times N}$ is given by,

$$A_{m,n}^{(f)} = \frac{e^{-j(2\pi f/c)r_{m,n}}}{4\pi r_{m,n}}. \tag{3.4}$$

The nth column of the matrix $\mathbf{A}^{(f)}$, $\mathbf{a}_n^{(f)}$, is the replica vector, which reflects the transmission from the nth potential noise source to the hydrophones.

In the localization method, let the incipient TVC noise comprise K-sparse sources; then, the incipient TVC localization problem is to find the actual locations of K noise sources among the assumed N locations ($K \ll N$). Equivalently, it is to find a linear combination of K-sparse bases (columns) out of *a priori* N bases in the sensing matrix $\mathbf{A}^{(f)}$.

3.2.2 Incoherent multiple-frequency localization with compressive sensing

As the noise source from the incipient TVC has a broadband frequency spectrum, we can utilize multiple-frequency measurements. Multiple-frequency processing exploring all the multiple-frequency measurements is an intuitive way to improve the localization performance.

For single-frequency processing, the incipient TVC localization problem is to recover a linear combination of K-sparse bases (columns) in *a priori* N bases of the sensing matrix $\mathbf{A}^{(f)}$, Eq. (4.3). Equivalently, it is to recover a sparse solution $\mathbf{x}$. CS recovers a sparse solution by minimizing the sparsity-enforcing norm (l_1-norm), $i.e.$, $\|\mathbf{x}\|_1 = \sum_{n=1}^{N}|x_n|$.

The incipient TVC localization problem using a single-frequency CS can be solved by the following the l_1-norm minimization problem,

$$\min_{\hat{\mathbf{x}}^{(f)}\in\mathbb{C}^N} \|\hat{\mathbf{x}}^{(f)}\|_1 \ \text{ subject to } \ \|\hat{\mathbf{y}}^{(f)} - \hat{\mathbf{A}}^{(f)}\hat{\mathbf{x}}^{(f)}\|_2 \le \hat{\epsilon}, \tag{3.5}$$

where $\hat{\mathbf{y}}^{(f)}$ and $\hat{\mathbf{a}}_n^{(f)}$ are normalized versions of $\mathbf{y}^{(f)}$ and $\mathbf{a}_n^{(f)}$, $i.e.$, $\hat{\mathbf{y}}^{(f)} = \mathbf{y}^{(f)}/\|\mathbf{y}^{(f)}\|_2$ and $\hat{\mathbf{a}}_n^{(f)} = \mathbf{a}_n^{(f)}/\|\mathbf{a}_n^{(f)}\|_2$. The nth entry of $\hat{\mathbf{x}}^{(f)}$ is $(\|\mathbf{a}_n\|_2/\|\mathbf{y}\|_2)x_n$. The normalization causes the candidate bases in $\mathbf{A}$ to have the same Euclidean norm, such that it prevents the bias induced by different distances $r_{m,n}$. [4, 8] $\hat{\epsilon}$ is the error floor that controls the error between measurements and the obtained results with respect to the l_2-norm. With large $\hat{\epsilon}$, we can obtain a very sparse solution permitting a large amount of error with poor data fit. With small $\hat{\epsilon}$, the resulting solution follows the measured data closely with overfitting, and it is not likely to have a sparse representation.

To utilize multiple frequencies of incipient TVC, incoherent multiple-frequency processing with CS can be used where single-frequency processing solutions across the multiple frequencies are applied individually and provide a more stable estimation. Incoherent multiple-frequency processing with CS involves obtaining a sparse solution at each single frequency, Eq. (3.5), and taking an average over the obtained sparse solutions,

$$\hat{\mathbf{x}}_{\text{incoh}} = \frac{1}{L}\sum_{l=1}^{L}|\hat{\mathbf{x}}^{(f_l)}|, \tag{3.6}$$

where f_l is the lth frequency for L frequencies in the TVC frequency spectrum. Then estimated amplitude of nth potential source which averaged across frequencies can be written as

$$s_{n,incoh} = \hat{x}_{n,\text{incoh}} \tag{3.7}$$

where $\hat{x}_{n,\text{incoh}}$ stands for nth entry of solution $\hat{\mathbf{x}}_{\text{incoh}}$ in Eq. (3.6). Therefore, source locations can be estimated by seeking for the non-zero $s_{n,incoh}$ value.

Note that the corresponding solution $\hat{\mathbf{x}}$ becomes less sparse if the single-frequency solutions $\hat{\mathbf{x}}^{(f_l)}$ do not share the non-zero components at the same locations. To take ad-

vantage of incoherent multiple-frequency processing, the conditions for single-frequency localization has to be satisfied; that is, high SNR, sufficient length of time-sample data, or sufficient number of frequencies is required.

3.2.3 Coherent multiple-frequency localization with block-sparse compressive sensing

The multiple-frequency CS-based incipient TVC localization problem can be solved using coherent multiple-frequency processing with CS. To better understand the coherent multiple-frequency CS structure, we provide an explanation of the multiple measurement vector (MMV) problem. [10, 24, 25] The MMV problem recovers the joint sparse source signals from a set of L measurement vectors. These vectors share the same non-zero support, which promotes spatial sparsity; thus, the signal can be reconstructed with high resolution. With L measurement vectors, this MMV model can be expressed as below,

$$\mathbf{Y} = \mathbf{A}\mathbf{X} + \mathbf{N} \tag{3.8}$$

where the MMVs $\mathbf{Y} \in \mathbb{C}^{M\times L}$, the sensing matrix $\mathbf{A} \in \mathbb{C}^{M\times N}$, and the N potential vectors $\mathbf{X} \in \mathbb{C}^{N\times L}$. For stationary sources, this approach can be utilized to enhance the localization performance. However, since vortex cavitation is a short-duration noise source of broadband, the MMV model is not appropriate for the localization method. Instead of the MMV problem, we introduce the multiple-frequency measurement vector, which promotes spatial sparsity.

Each single-frequency sparse model, Eq. (3.5), uses a different sensing matrix for each frequency; thus, MMV formation cannot be utilized for the multiple frequency measurement vectors. To use multiple-frequency measurement vectors, block-sparse CS is utilized to combine the set of the single-frequency sparse models into a block-sparse model, as shown in Fig. 3.1, $i.e.$, multiple-frequency measurement vectors are

combined into a single vector.

With this concept and L frequencies $(f_1, \cdots, f_L)$ in the TVC frequency spectrum, we can extend the normalized version of the sparse measurement model, $\hat{\mathbf{y}}^{(f)} = \hat{\mathbf{A}}^{(f)}\hat{\mathbf{x}}^{(f)}$, as a block-sparse measurement model,

$$\tilde{\mathbf{y}} = \tilde{\mathbf{A}}\tilde{\mathbf{x}} + \tilde{\mathbf{n}}, \tag{3.9}$$

where multiple-frequency measurement vector $\tilde{\mathbf{y}} \in \mathbb{C}^{ML}$, sensing matrix of block-sparse model $\tilde{\mathbf{A}} \in \mathbb{C}^{ML \times NL}$ (M: number of receivers, N: number of potential sources, L: number of frequencies). Multiple-frequency measurement vector $\tilde{\mathbf{y}}$ and block-sparse vector $\tilde{\mathbf{x}} \in \mathbb{C}^{NL}$ take the forms,

$$\begin{aligned}\tilde{\mathbf{y}} &= [\tilde{\mathbf{y}}_1^{\text{block}}; \cdots; \tilde{\mathbf{y}}_M^{\text{block}}] \\ &= [\underbrace{\tilde{y}_1^{(f_1)}, \cdots, \tilde{y}_1^{(f_L)}}_{\tilde{\mathbf{y}}_1^{\text{block}}}, \cdots, \underbrace{\tilde{y}_M^{(f_1)}, \cdots, \tilde{y}_M^{(f_L)}}_{\tilde{\mathbf{y}}_M^{\text{block}}}]^{\mathsf{T}},\end{aligned} \tag{3.10}$$

$$\begin{aligned}\tilde{\mathbf{x}} &= [\tilde{\mathbf{x}}_1^{\text{block}}; \cdots; \tilde{\mathbf{x}}_N^{\text{block}}] \\ &= [\underbrace{\tilde{x}_1^{(f_1)}, \cdots, \tilde{x}_1^{(f_L)}}_{\tilde{\mathbf{x}}_1^{\text{block}}}, \cdots, \underbrace{\tilde{x}_N^{(f_1)}, \cdots, \tilde{x}_N^{(f_L)}}_{\tilde{\mathbf{x}}_N^{\text{block}}}]^{\mathsf{T}},\end{aligned} \tag{3.11}$$

and

$$\tilde{\mathbf{A}} = \begin{bmatrix} \tilde{\mathbf{A}}_{1,1}^{\text{block}} & \cdots & \tilde{\mathbf{A}}_{1,N}^{\text{block}} \\ \vdots & \ddots & \vdots \\ \tilde{\mathbf{A}}_{M,1}^{\text{block}} & \cdots & \tilde{\mathbf{A}}_{M,N}^{\text{block}} \end{bmatrix}, \tag{3.12}$$

where $\tilde{\mathbf{A}}_{m,n}^{\text{block}}$ is the (m,n)th partition of the matrix $\tilde{\mathbf{A}}$,

$$\tilde{\mathbf{A}}_{m,n}^{\text{block}} = \text{diag}\left(\hat{a}_{m,n}^{(f_1)}, \cdots, \hat{a}_{m,n}^{(f_L)}\right) = \begin{bmatrix} \hat{a}_{m,n}^{(f_1)} & 0 & \cdots & 0 \\ 0 & \hat{a}_{m,n}^{(f_2)} & \cdots & 0 \\ \vdots & \vdots & \ddots & \vdots \\ 0 & 0 & \cdots & \hat{a}_{m,n}^{(f_L)} \end{bmatrix}, \tag{3.13}$$

and $\hat{a}_{m,n}^{(f_l)}$ is the (m,n)th entry of the matrix $\hat{\mathbf{A}}^{(f_l)}$ in Eq. (3.5). Note that the solution $\tilde{\mathbf{x}}$ is blockwise sparse.

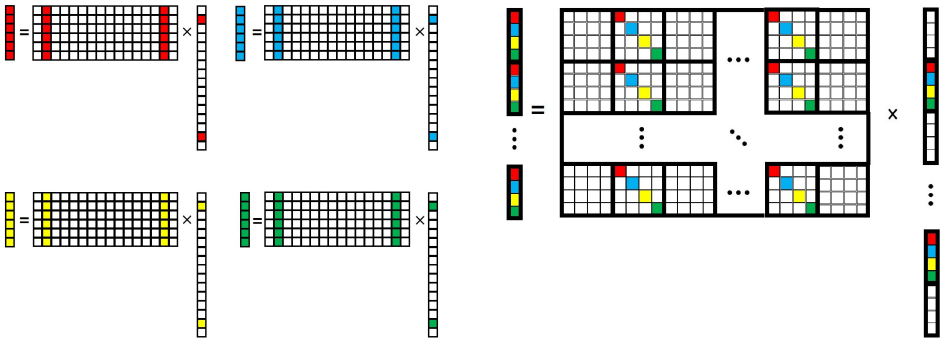

(a) Incoherent processing (b) Coherent processing

Figure 3.1: (Color online) (a) Conventional compressive sensing (CS) model with multiple measurement vectors (MMV). Each color indicates temporal difference and the non-zero components in the measurement vectors share the same dictionaries because they are temporally correlated (sparsity level is two) and (b) block-sparse CS model for coherent multiple-frequency processing. Each color indicates frequency difference and the non-zero components in the measurement vector correspond to the different dictionaries because they are uncorrelated (block-sparsity level is two).

In Eq. (4.27), we can infer that the unknown parameters to be solved have been increased from N to NL. This means that if there are K-sparse sources, we should solve KL sparse problem. Fortunately, a few sources that have broadband characteristics can

be expressed as block-sparse $\tilde{\mathbf{x}}$; thus, we can utilize the block-sparse CS to solve the more optimal K-sparse problem than the KL-sparse problem. As $\tilde{\mathbf{x}}$ is K-block-sparse, the localization problem is to find a combination of K-sparse column-blocks in *a priori* N column-blocks of the block-sparse sensing matrix $\tilde{\mathbf{A}}$.

To solve the K-block-sparse system, we use an l_2/l_1-norm minimization technique [8] to find the nonzero blocks. Just as the l_1-norm minimization technique [3] used in conventional CS, l_2/l_1-norm minimization technique minimizes the sum of the l_2-norm of the blocks.

Then, the incipient TVC localization with block-sparse CS is solved using the following formulation:

$$\min_{\tilde{\mathbf{x}}\in\mathbb{C}^{NL}} \sum_{n=1}^{N} \|\tilde{\mathbf{x}}_n^{\text{block}}\|_2 \;\text{ subject to }\; \|\tilde{\mathbf{y}} - \tilde{\mathbf{A}}\tilde{\mathbf{x}}\|_2 \leq \tilde{\epsilon}, \tag{3.14}$$

where $\tilde{\mathbf{x}}_n^{\text{block}} = \left[\tilde{x}_n^{(f_1)}, \cdots, \tilde{x}_n^{(f_L)}\right]^{\mathsf{T}}$ and $\tilde{\epsilon}$ is the error floor, in which the role is similar to that of $\hat{\epsilon}$ in Eq. (3.5). Note that sparsity is imposed on the l_2-norm of the blocks of vector $\tilde{\mathbf{x}}$.

Referring to Eq. (3.5) and Eq. (3.14), the dimension of unknown vector to be reconstructed have been increased $\mathbf{x}^{(f)} \in \mathbb{C}^N$ to $\tilde{\mathbf{x}} \in \mathbb{C}^{NL}$, where $\tilde{\mathbf{x}}$ is a block-sparse vector.

We considered the problem of reconstructing a block-sparse vector that represents the broadband acoustic sources. As these sources are sparse and broadband, entries of the block corresponding to real source positions will all be nonzero. Thus, the problem of using block-sparse CS will not increase the sparsity, even though the number of unknown parameters are increased but rather enhance the sparsity. [8]

To localize the TVC sources, we consider the case of only a few broadband sources, $i.e.$, $\tilde{\mathbf{x}}$ is block-sparse. We assume that the TVC sources are sparse; thus, the spatial candidates (number of potential sources) are not increased compared with the number of incoherent parameters (number of potential sources). This means that the increased

number of unknown parameters do not increase the sparsity ($i.e.$, block-sparsity) for this problem. As expressed in Eq. (3.14), we search for candidates representing the real source signal. Using the block-sparse concept, this means that certain potential sources radiate a broadband signal, rather than a tonal signal, and signal vectors will be reconstructed only with fully filled blocks or fully blank blocks. Therefore, amplitude of nth potential source for coherent multiple-frequency processing can be written as

$$s_{n,coh} = ||\tilde{\mathbf{x}}_n^{\text{block}}||_2 \tag{3.15}$$

where $\tilde{\mathbf{x}}_n^{\text{block}}$ stands for nth block of solution $\tilde{\mathbf{x}}$ in Eq. (4.27) and source locations can be estimated by seeking for the non-zero $s_{n,coh}$ value.

3.3 Localization Results for Incipient TVC

In this section, we apply the block-sparse CS to measurement data from the cavitation tunnel experiments for incipient TVC localization. Two experiments were conducted with a transducer source (known source position) and an incipient TVC noise source. For a localization search grid with potential noise sources, the potential sources are evenly distributed near the true source location at a 0.05 m interval for the transducer source case and a 0.01 m interval for the incipient TVC noise source case. The objective of the transducer source experiment is to validate the block-sparse CS localization algorithm and compare the localization results from coherent multiple-frequency processing to those from incoherent multiple-frequency processing. The objective of the incipient TVC noise source experiment is to demonstrate the high-resolution capabilities and robustness of the block-sparse CS in the incipient TVC localization.

3.3.1 Transducer source experiment

The high-resolution performance of block-sparse CS, coherent multiple-frequency processing, is validated with experimental data from cavitation tunnel experiments, and it is compared with conventional CS and incoherent multiple-frequency processing.

The configuration of the transducer source experiment is shown in Fig. 3.2(a). One transducer source (ITC-1001) with known location information was located in the cavitation tunnel and was transmitting a broadband signal, whose spectrum ranged from 7 to 37 kHz. The data set was collected on $M = 6$ hydrophones (B&K 8103) mounted beneath the upper part of the cavitation tunnel. Here, we set the potential transducer noise sources (the localization search grid) to be evenly distributed near the true source location with a 0.05 m interval over a three-dimensional volume (x-axis: -0.5–0.5 m, y-axis: -1.4–0 m, z-axis: -1.5–1.5 m), $i.e.$, the number of candidates $N = 37,149$ ($21 \times 29 \times 61$).

Coherent multiple-frequency processing with block-sparse CS is compared to incoherent multiple-frequency processing with conventional CS [4], as shown in Fig. 3.3. Here, we use $L = 10$ frequencies ([7, 10, 13, 16, 19, 22, 25, 28, 31, 34] kHz). We have chosen error floors $\hat{\epsilon}$ $\big($Eq. (3.5)$\big)$ and $\tilde{\epsilon}$ $\big($Eq. (3.14)$\big)$ for the results to have a sparsity level of three. Coherent multiple-frequency processing estimates the true location of the transducer source with one significant component, but incoherent multiple-frequency processing fails to localize the source.

The localization performance of incoherent multiple-frequency processing can be improved by processing many frequency components, as shown in Fig. 3.4. The number of processed frequencies varies from $L = 30$ $\big($Fig. 3.4(b)$\big)$ to $L = 120$ $\big($Fig. 3.4(d)$\big)$ in the 7–37 kHz frequency band. Incoherent multiple-frequency processing with conventional CS requires a sufficient number of meaningful single-frequency processing solutions that localize the true source location. Still, even though a number of frequencies are considered as in Fig. 3.4(d), the dominant source, which character-

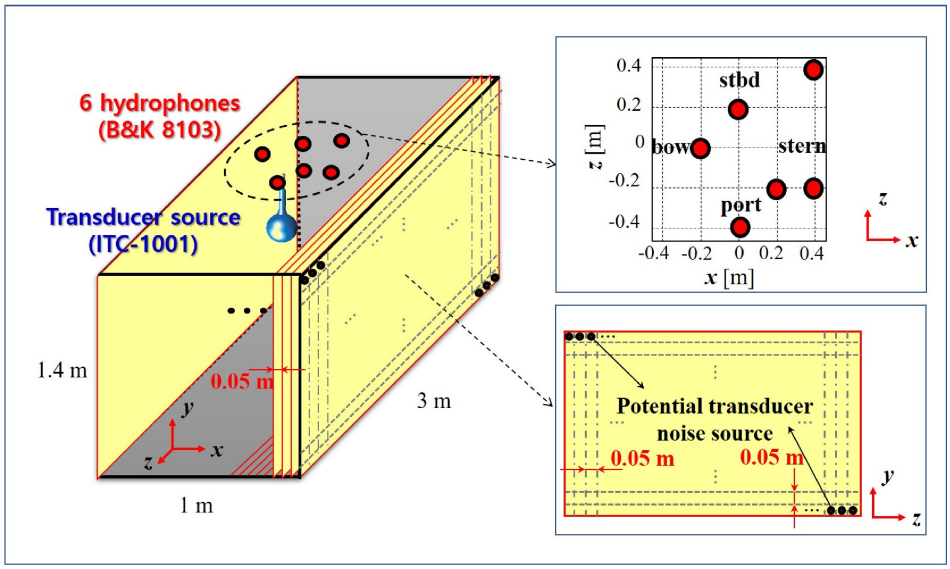

(a) Transducer source experiment

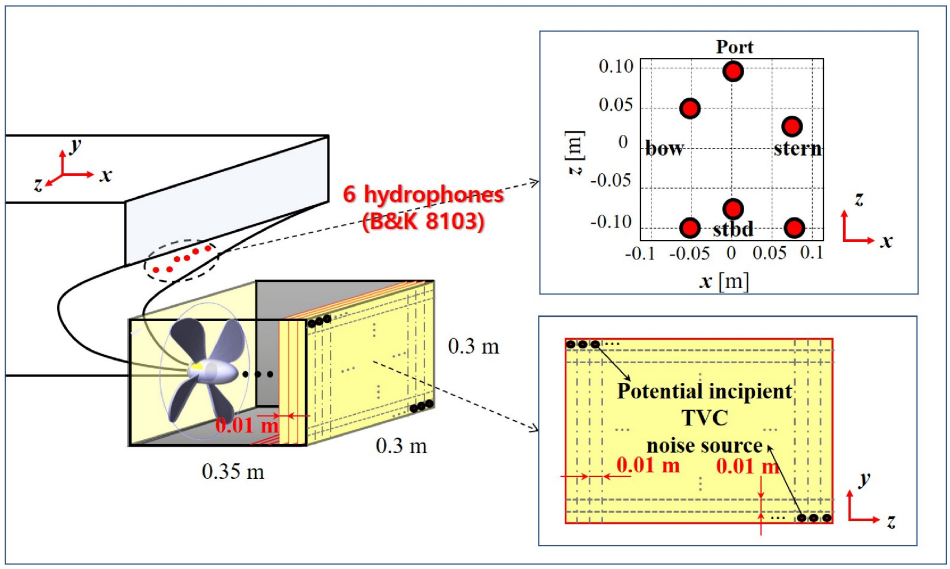

(b) Cavitation source experiment

Figure 3.2: (Color online) Schematic plan of hydrophones and potential noise sources (search grid) for (a) the transducer source experiment and (b) the incipient tip vortex cavitation (TVC) source experiment.

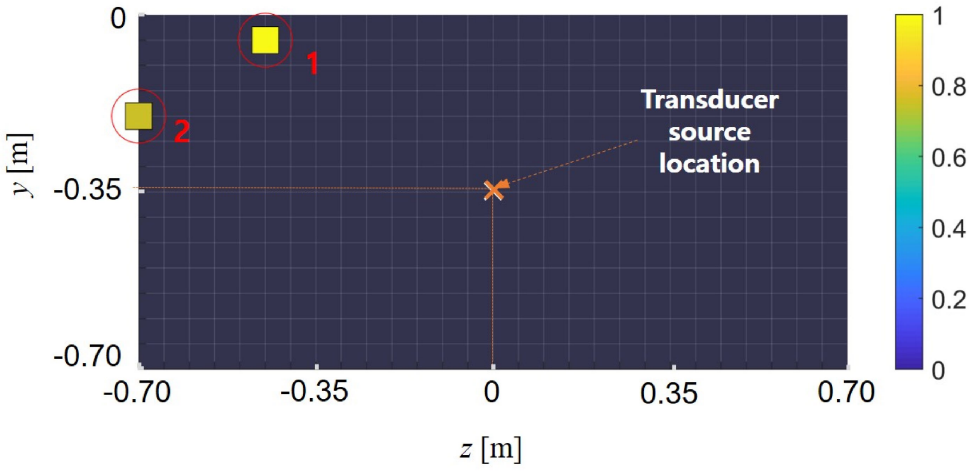

(a) Incoherent multiple-frequency processing

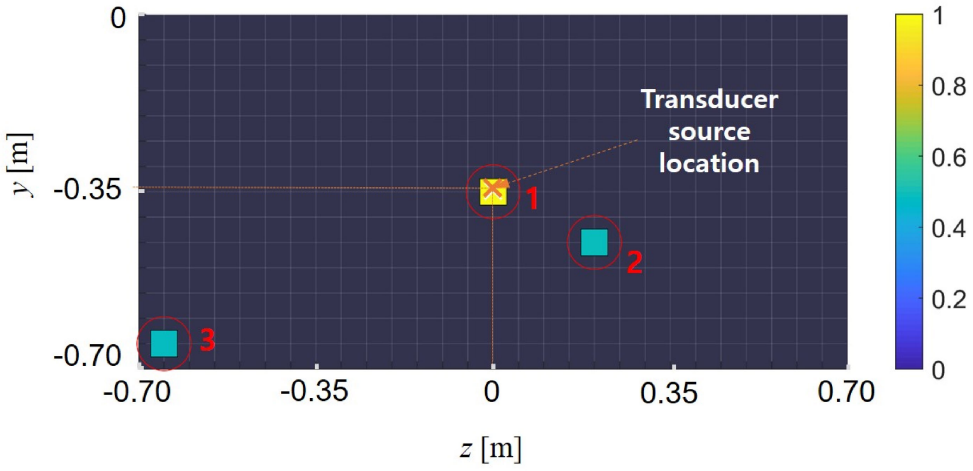

(b) Coherent multiple-frequency processing

Figure 3.3: (Color online) Source localization with experimental data for the transducer source, of which location is known, with (a) conventional CS (incoherent multiple-frequency processing) and (b) block-sparse CS (coherent multiple-frequency processing) on the y-z plane at a fixed $x = 0$ m. The three largest source amplitudes (Eq. (3.7) and Eq. (3.15)) are plotted and each amplitude are normalized to maximum amplitude of one.

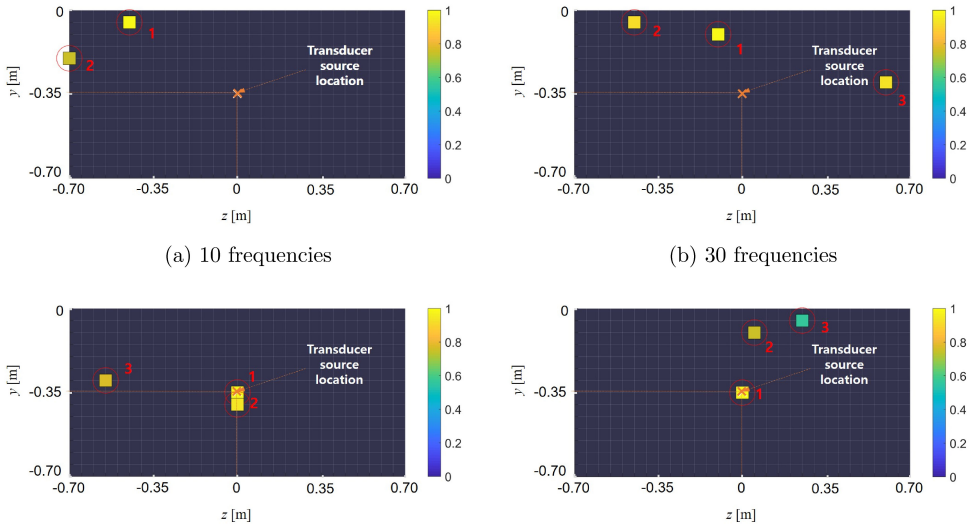

(a) 10 frequencies

(b) 30 frequencies

(c) 60 frequencies

(d) 120 frequencies

Figure 3.4: (Color online) Same as Fig. 3.3., except for incoherent processing with different numbers of processed frequencies.

izes the overall multiple-frequency pressure field, is not noticeably distinguished from the other candidates without sufficiently high SNR. Note that this localization can be regarded as 1-sparse problem. However, it is apparent from Fig. 3.3 and Fig. 3.4. that incoherent multiple-frequency processing cannot provide stable localization result without sufficiently high SNR and without a sufficient number of measurement information.

3.3.2 Incipient TVC Noise Source Experiment

In this section, block-sparse CS for incipient TVC localization is applied to the experimental data from the cavitation tunnel experiment. The configuration of the incipient TVC source experiment is shown in Fig. 3.2(b). The data set was collected on $M = 6$ hydrophones (B&K 8103) mounted on the hull surface of the model ship above the propeller.

Incipient TVC is observed at the top center of the propeller near the propeller tip,

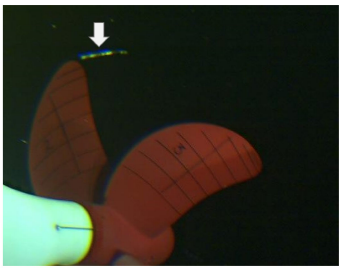

(a) Visual observation

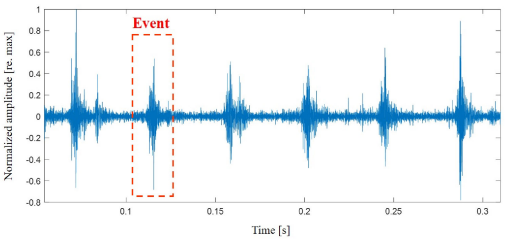

(b) Acoustical observation

Figure 3.5: (Color online) (a) Visual observation of TVC and (b) measured acoustic data in the incipient TVC stage. The acoustic data in the time domain is bandpass-filtered (20-50 kHz).

as shown in Fig. 3.5(a). Noise induced by the incipient TVC is emitted in all directions and can be modeled as a monopole source. [6] The TVC noise has a broadband frequency spectrum, [1] and bandpass-filtered (20–50 kHz) acoustic measurement data in the time domain is shown in Fig. 3.5(b). Readers are referred to Refs. [4, 6] for detailed discussions on the experimental configuration.

Here, we set the potential TVC noise sources (the localization search grid) to be evenly distributed near the top center of the propeller with a 0.01 m interval over a three-dimensional volume (x-axis: -0.05–0.3 m, y-axis: -0.15–0.15 m, z-axis: -0.15–0.15 m), $i.e.$, the number of candidates $N = 34,596$ ($36 \times 31 \times 31$). We have chosen the error floors $\hat{\epsilon}$ $\big($Eq. (3.5)$\big)$ and $\tilde{\epsilon}$ $\big($Eq. (3.14)$\big)$ for the results to have a sparsity level of three (here, we manually selected error floor for 0.3). Then, we have solved Eq. (3.5) and Eq. (3.14) by utilizing the CVX toolbox [37].

Table 3.1. shows the numerical results for the coherent multiple-frequency processing and the incoherent multiple-frequency processing. To examine the localization performance for multiple noise sources, localization errors between simulated sources and estimated sources are analyzed comparing the coherent multiple-frequency processing with the incoherent multiple-frequency processing. We generated randomly

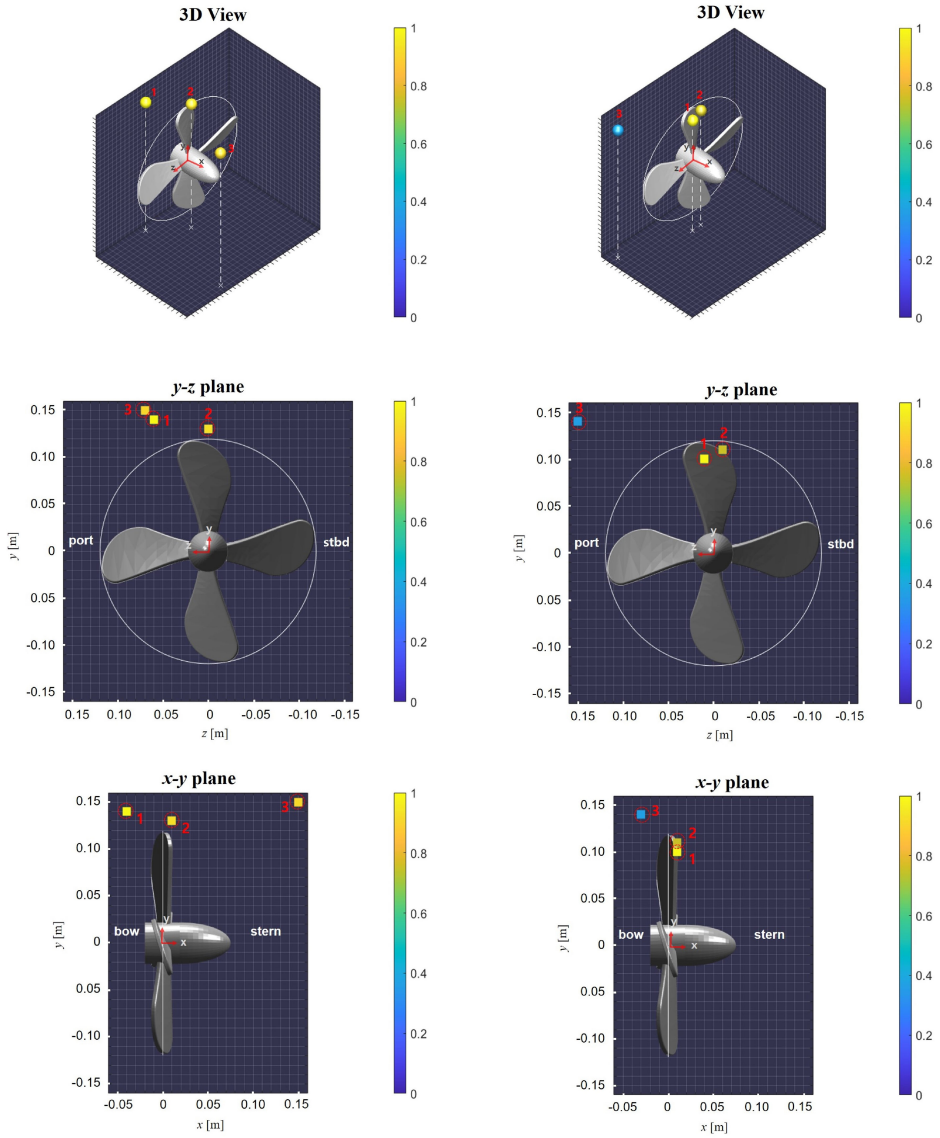

(a) Incoherent multiple-frequency processing (b) Coherent multiple-frequency processing

Figure 3.6: (Color online) Source localization with experimental data for the cavitation source with (a) conventional CS (incoherent multiple-frequency processing) and (b) block-sparse CS (coherent multiple-frequency processing). The three largest source amplitudes (Eq. (3.7) and Eq. (3.15)) are plotted and each amplitude are normalized to maximum amplitude of one.

Table 3.1: Mean localization error simulation result in terms of sparsity level. The source numbers are sorted from large to small amplitude (source 1 is the largest one).

Case	**Coherent processing**			**Incoherent processing**		
	Source 1	Source 2	Source 3	Source 1	Source 2	Source 3
Sparsity = 1	0.0004 m	-	-	0.0003 m	-	-
Sparsity = 2	0.0019 m	0.0039 m	-	0.1151 m	0.1513 m	-
Sparsity = 3	0.0176 m	0.0203 m	0.0299 m	0.1338 m	0.1674 m	0.1796 m

distributed (on the search grids) monopole sources with random amplitudes (normalized between 0.5 and 1.0) and random phases ([0-2π]) over selected frequencies ([20 : 2.5 : 50] kHz). The number of generated monopole sources are selected according to the sparsity level (= 1-3). Complex Gaussian noise is added to the measurement with a 20 dB signal-to-noise ratio (which is similar to that of the cavitation measurement data) and the rest of simulation setup is the same as real TVC experimental configuration. Then the localization was conducted for each processing and localization errors were estimated in terms of the number of the sources (=sparsity level) as illustrated in Table 3.1. It is apparent from Table 3.1. that coherent multiple-frequency processing is accurate over various sparsity levels (note that spatial grid is evenly distributed with a 0.01 m interval) and localization errors grow as the sparsity level increases. We can infer that coherent multiple-frequency processing has the capability to distinguish spatially separate sources. However, incoherent multiple-frequency processing only works in the case of sparsity level 1. This means that incoherent multiple-frequency processing is not the proper method for multiple-source localization problem.

Then, the processes are applied to experimental TVC data and coherent multiple-frequency processing with block-sparse CS $\big($Fig. 3.6(b)$\big)$ is compared to incoherent multiple-frequency processing with conventional CS [4] $\big($Fig. 3.6(a)$\big)$. As incoherent multiple-frequency processing requires a sufficient number of frequencies to be processed, different numbers of frequencies are considered: $L = 13$ frequencies

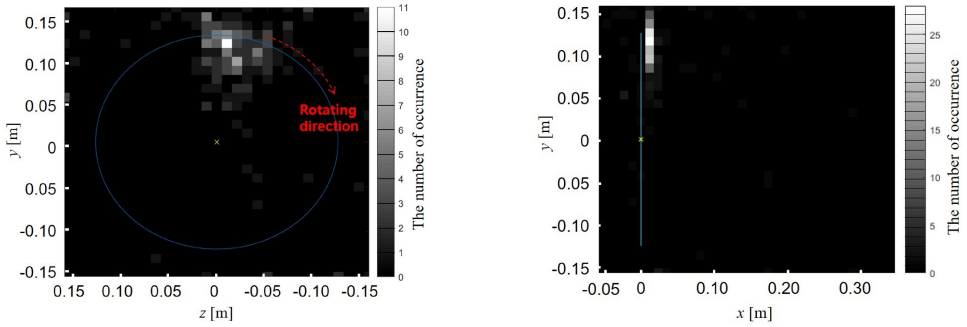

(a) y-z plane (b) x-y plane

Figure 3.7: (Color online) Histogram of the locations of the largest estimated sources for 200 cavitation events on (a) the y-z plane at a fixed $x = 0$ m and (b) the x-y plane at a fixed $z = 0$ m.

([20 : 2.5 : 50] kHz) for coherent multiple-frequency processing and $L = 121$ frequencies ([20 : 0.25 : 50] kHz) for incoherent multiple-frequency processing.

Coherent multiple-frequency processing estimates two locations around the top center of the propeller and at the downstream direction (Fig. 3.6(b)). Because the tip vortex line is induced at the back of the propeller, the localization result corresponds to the visual observation (Fig. 3.5(a)). In contrast, incoherent multiple-frequency processing fails to estimate a dominant location, and it localizes one near the top of the propeller but with the second largest component (Fig. 3.6(a)).

Fig. 3.7. shows the distribution of the largest components of the localization results for 200 cavitation events (Fig. 3.5(b)). The localization results are concentrated around the top center of the propeller (Fig. 3.7(a)) and at the downstream direction (Fig. 3.7(b)). Note that, the variability of the estimated locations in the x-axis is small.

The multiple-frequency data with block-sparse CS reveals that block-sparse CS enables coherent multiple-frequency processing over multiple frequencies and acoustically localizes the TVC noise source in accordance with the visual signature of the TVC.

3.4 Conclusion

The purpose of this section is to localize the incipient TVC noise sources via block-sparse CS. CS is applied in the sparse nature of the TVC noise sources. Given that TVC noise radiates a broadband signal, multiple-frequency processing improves performance in localization over single-frequency processing. For coherent multiple-frequency processing, which jointly considers the measured data at multiple frequencies, block-sparse CS is utilized.

In contrast to incoherent multiple-frequency processing using conventional CS, coherent multiple-frequency processing provides accurate localization results, even with a fewer number of processed frequencies. Also, coherent multiple-frequency processing does not need long-time-sampled data with a time-invariant signal assumption to obtain high resolution in incoherent multiple-frequency processing.

The real data results indicate that the block-sparse CS is capable of localizing the incipient TVC noise sources, and the estimated locations correspond with the visual observations of TVC.

Table 3.2: Summary of the proposed method

Coherent Multiple-frequency Processing	
Methodologies	• Block-spare compressive sensing(BSCS) • Convex optimization(l_2/l_1-norm minimization) • Promoting the joint sparse property
Advantages	• High-resolution localization results • Noise robustness
Limitations	• Vulnerable to basis mismatch error • Fine spatial grid points are required

3.5 Acknowledgments

This chapter, in full, is a reprint of the material as it appears in The Journal of the Acoustical Society of America, 2020, with authors M. Park, Y. Park, K. Lee. and W. Seong. Reprinted with permission from M. Park, Y. Park, K. Lee. and W. Seong, "Incipient tip vortex cavitation localization using block-sparse compressive sensing," J. Acoust. Soc. Am. 147(5), 3454-3464 (2020).

References

[1]Y. Lecoffre, *Cavitation: bubble trackers* (Balkema, Leiden, 1999) Chap. 8 and 9, pp. 140–210.

[2]A. Tolstoy, *Matched field processing for underwater acoustics* (World Scientific Publishing, Singapore, 1993) Chap. 4, pp. 91–180.

[3]D. L. Donoho, "Compressed sensing", IEEE Trans. Inf. Theory **52**, 1289–1306 (2006).

[4]Y. Choo and W. Seong, "Compressive spherical beamforming for localization of incipient tip vortex cavitation", J. Acoust. Soc. Am. **140**, 4085–4090 (2016).

[5]C. Park, H. Seol, K. Kim, and W. Seong, "A study on propeller noise source localization in a cavitation tunnel", Ocean Eng. **36**, 754–762 (2009).

[6]D. Kim, W. Seong, Y. Choo, and J. Lee, "Localization of incipient tip vortex cavitation using ray based matched field inversion method", J. Sound Vib. **354**, 34–46 (2015).

[7]C. Park, G. Kim, Y. Park, K. Lee, and W. Seong, "Noise localization method for model tests in a large cavitation tunnel using a hydrophone array", Remote Sens. **8**, 195 (2016).

[8]Y. C. Eldar, P. Kuppinger, and H. Bolcskei, "Block-sparse signals : uncertainty relations and efficient recovery", IEEE Trans. Signal Process. **58**, 3042–3054 (2010).

[9]R. G. Baraniuk, V. Cevher, M. F. Duarte, and C. Hegde, "Model-based compressive sensing", IEEE Trans. Inf. Theory **56**, 1982–2001 (2010).

[10]J. Tropp, A. C. Gilbert, and M. J. Strauss, "Algorithms for simultaneous sparse approximation. part i: greedy pursuit", Signal Processing **86**, 572–588 (2006).

[11]M. Yuan and Y. Lin, "Model selection and estimation in regression with grouped variables", J. Acoust. Soc. Am. **68**, 49–67 (2006).

[12]N. A. Chang and D. R. Dowling, "Ray-based acoustic localization of cavitation in a highly reverberant environment", J. Acoust. Soc. Am. **125**, 3088–3100 (2009).

[13]N. A. Chang and S. L. Ceccio, "The acoustic emissions of cavitation bubbles in stretched vortices", J. Acoust. Soc. Am. **130**, 3209–3219 (2011).

[14]K. Lee, J. Lee, D. Kim, K. Kim, and W. Seong, "Propeller sheet cavitation noise source modeling and inversion", J. Sound Vib. **333**, 1356–1368 (2014).

[15]D. Kim, K. Lee, and W. Seong, "Non-cavitating propeller noise modeling and inversion", J. Sound Vib. **333**, 6424–6437 (2014).

[16]D. Malioutov, M. Cetin, and A. Willsky, "A sparse signal reconstruction perspective for source localization with sensor arrays", IEEE Trans. Signal Process. **53**, 3010–3022 (2005).

[17]A. Xenakia and P. Gerstoft, "Compressive beamforming", J. Acoust. Soc. Am. **136**, 260–271 (2014).

[18]N. Wagner, Y. C. Eldar, and Z. Friedman, "Compressed beamforming in ultrasound imaging", IEEE Trans. Signal Process. **60**, 4643–4657 (2012).

[19]C. Yardim, P. Gerstoft, W. S. Hodgkiss, and J. Traer, "Compressive geoacoustic inversion using ambient noise", J. Acoust. Soc. Am. **135**, 1245–1255 (2014).

[20]G. Chardon, L. Daudet, A. Peillot, F. Ollivier, N. Bertin, and R. Gribonval, "Near-field acoustic holography using sparse regularization and compressive sampling principles", J. Acoust. Soc. Am. **132**, 1521–1534 (2012).

[21]E. Fernandez-Grande, A. Xenaki, and P. Gerstoft, "A sparse equivalent source method for near-field acoustic holography", J. Acoust. Soc. Am. **141**, 532–542 (2017).

[22]C. X. Bi, Y. Liu, L. Xu, and Y. Zhang, "Sound field reconstruction using compressed modal equivalent point source method", J. Acoust. Soc. Am. **141**, 73–79 (2017).

[23]P. A. Forero and P. A. Baxley, "Shallow-water sparsity-cognizant source-location mapping", J. Acoust. Soc. Am. **135**, 3483–3501 (2014).

[24]P. Gerstoft, A. Xenaki, and C. F. Mecklenbrauker, "Multiple and single snapshot compressive beamforming", J. Acoust. Soc. Am. **138**, 2003–2014 (2015).

[25]S. F. Cotter, B. D. Rao, K. Engan, and K. Kreutz-Delgado, “Sparse solutions to linear inverse problems with multiple measurement vectors”, IEEE Trans. Signal Process. **53**, 2477–2488 (2005).

[26]Y. Park, Y. Choo, and W. Seong, “Multiple snapshot grid free compressive beamforming”, J. Acoust. Soc. Am. **143**, 3849–3859 (2018).

[27]R. Tibshirani and J. Taylor, “The solution path of the generalized lasso”, Annals Stat. **39**, 1335–1371 (2011).

[28]A. Xenaki, E. Fernandez-Grande, and P. Gerstoft, “Block-sparse beamforming for spatially extended sources in a bayesian formulation”, J. Acoust. Soc. Am. **140**, 1828–1838 (2016).

[29]E. Fernandez-Grande and L. Daudet, “Compressive acoustic holography with block-sparse regularization”, J. Acoust. Soc. Am. **143**, 3737–3746 (2014).

[30]Y. Park, Y. Choo, and P. Gerstoft, “Block-sparse two-dimensional off-grid beamforming with arbitrary planar array geometry”, J. Acoust. Soc. Am. **147**, 2184–2191 (2020).

[31]M. E. Tipping, “Sparse bayesian learning and the relevance vector machine”, J. Mach. Learn. Res. **1**, 211–244 (2001).

[32]D. P. Wipf and B. Rao, “An empirical bayesian strategy for solving the simultaneous sparse approximation problem”, IEEE Trans. Signal Process. **55**, 3704–3716 (2007).

[33]P. Gerstoft, C. Mecklenbrauker, A. Xenaki, and S. Nannuru, ““multi-snapshot sparse bayesian learning for doa””, IEEE Signal Process. Letters **23**, 1469–1473 (2016).

[34]Z. Zhang and B. Rao, “Sparse signal recovery with temporally correlated source vectors using sparse bayesian learning”, IEEE J. Sel. Topics Signal Process. **5**, 912–926 (2011).

[35]J. Choi and G. L. Chahine, “Noise due to extreme bubble deformation near inception of tip vortex cavitation”, Phys. Fluids **16**, 2411–2418 (2004).

[36]J. Choi and S. L. Ceccio, "Dynamics and noise emission of vortex cavitation bubbles", J. Fluid Mech. **575**, 1–26 (2007).

[37]M. Grant, S. Boyd, and Y. Ye, *CVX: matlab software for disciplined convex programming, version 2.1*, (Last viewed April 11, 2019), 2008.

Chapter 4

3D CS-based source localization method by reducing the basis mismatch error

4.1 Introduction

Three-dimensional acoustic source localization is a trivial problem in underwater acoustics since the received signals are superposed induced by the acoustic sources. To track each acoustic source location, the received signal should be properly decomposed to several source components and noise components, however, several mismatch factors(such as reverberation, heavy noise, multi-path effect) hinder the accurate estimation. Thus, effective signal processing which reducing the mismatch error is essentially required for localizing the accurate source positions. Compressive sensing based approach is an effective way to reconstruct acoustic source information. However, the processing is conducted in discretized bases, basis mismatch error should be occured. Although off-grid approaches, which prevent the basis mismatch error, were proposed to acoustic source localization problems, the approaches are only applicable to the 1-dimensional problems($e.g.$, DOA estimation problem) and the 2-dimensional problems($e.g.$, 2D plane-wave beamforming problem). In this paper, we suggest the off-grid approach using the SBL algorithm applicable to 3-dimensional problems. As

far As we know, this is the first 3-dimensional localization method which can resolve the basis-mismatch issue.

Localization of propeller cavitation is a representative 3d source localization problem in underwater acoustics. Cavitation emits broadband impulse signal and can be simply modeled as a few monopole type sources. In the case that noise merely exists, the traditional TDOA-based method, which is conventionally used in the source localization problem, can be an effective method to localize the cavitation. Chang and Dowling used the TDOA-based[1, 2] method and presented the cavitation localization results. However, they suffered from the effects of reverberation and used additional signal processing to obtain the direct-path signal. On the other hand, the MFP-based method [3–7] showed that accurate localization can be achieved despite the presence of the multi-path effect. However, these results provide only ambiguous information of source locations such as the ambiguity surface and the acoustic center, so that the results did not present the distinct source locations. CS is a signal reconstruction technique[8]
applicable to sufficiently sparse signals with less measurement data and has shown that it can be applied to the underlying acoustic models which have sparse representations in the basis.[9–15] The CS-based methods, applied to the cavitation localization problem[16, 17], showed enhanced performance with respect to resolution compared with the MFP-based methods. However, these CS-based localization processes were conducted in the discretized spatial grid points so that the basis mismatch error was not considered. To enhance the localization performance, reducing the basis mismatch error is essentially required. In this chapter, we present a off-grid technique which is applicable to the 3-dimensional localization problem based on the SBL(sparse Bayesian learning) approaches.

The SBL is a kind of compressive sensing technique which takes a probabilistic approach to reconstruct the sparse signal. [18] The SBL technique set the probabilistic

relationship between the measurement vector and the solution vector. Then, the SBL seeks for an optimized solution vector by maximizing the posterior. In underwater signal processing, the SBL technique had been widely used for source localization problem and had shown that it has better localization performance in terms of accuracy compared to the traditional localization methods.[19–22] The OGSBI [23] is a kind of the SBL based technique which reduces the basis mismatch error. Unlike the atomic norm minimization based approaches[24–26], OGSBI based approaches are robust to noise, have fewer global minima. For these reasons, We have studied OGSBI based off grid technique and suggest a CS-based localization method which works for 3-dimensional source localization problems.

One contribution of our study is that we firstly propose an off-grid localization method for spherical wave beamforming problems. To estimate the basis mismatch in the 3-dimensional space, we introduce flexible grid points which are varying with each iteration. Another contribution is providing the multi-frequency processing exploiting the BSBL approach. The Coherent multi-frequency processing[17] promotes spectral joint sparsity so that numerical instability can be resolved. We provide BSBL[27] based coherent multi-frequency processing which provides stable localization result for broadband sources.

The rest of this chapter is organized as follows. In Sec. 4.2, we propose an off-grid technique which can be applied to 3D source localization problems. Sec. 4.3 provides some simulated and experimental results to show the performance of the proposed approach. Finally, Sec. 4.4 provides the conclusion and contributions of the study.

4.2 Off grid system framework for 3D source localization

4.2.1 System framework for 3-dimensional off gird source localization

The broadband noise source transmits a monopole-type spherical waveform in all directions. Considering a single frequency f monopole source transmission, the re-

ceived signal through the direct path at the mth hydrophone $t_m^{(f)}$ can be derived as

$$t_m^{(f)} = \frac{e^{-j(2\pi f/c)r_m}}{4\pi r_m} w^{(f)} + n_m^{(f)}, \tag{4.1}$$

where $t_m^{(f)}$ is the measured sound pressure, c is the water sound speed, r_m is the distance from the cavitation noise source to the mth hydrophone, $w^{(f)}$ is a complex amplitude which has magnitude and initial phase of the cavitation noise, and $n_m^{(f)}$ is the error that involves electric noise, experimental error, or mismatch between actual phenomena and modeling.

In the localization problem, the search space is discretized by potential noise source locations, and the objective is to find the actual locations of the (usually few) noise sources among the assumed potential locations. Let $\mathbf{w}^{(f)} \in \mathbb{C}^N$ be an (sparse) unknown vector we aim to reconstruct, where N is the number of discretized potential locations of noise sources.

The measurement data at the mth hydrophone, which is the superposition of spherical waves from N potential sources, can be expressed using potential noise sources $\mathbf{w}^{(f)}$,

$$t_m^{(f)} = \sum_{n=1}^{N} \frac{e^{-j(2\pi f/c)r_{m,n}}}{4\pi r_{m,n}} w_n^{(f)} + n_m^{(f)}, \tag{4.2}$$

where $r_{m,n}$ is the distance from the mth hydrophone to the nth potential noise source, and the unknown vector $\mathbf{w}^{(f)}$ is composed of N complex amplitudes. Note that a fine resolution localization performance is desired; thus, $M \ll N$.

Then, the relationship between M hydrophones and N potential noise sources can be expressed as below

$$\mathbf{t}^{(f)} = \mathbf{A}^{(f)}\mathbf{w}^{(f)} + \mathbf{n}^{(f)}, \tag{4.3}$$

where $\mathbf{t}^{(f)}$ is the measurement vector at M hydrophones $\mathbf{t}^{(f)} \in \mathbb{C}^M$, and the (m,n)th entry of the matrix $\mathbf{A}^{(f)} \in \mathbb{C}^{M\times N}$ is given by,

$$A_{m,n}^{(f)} = \frac{e^{-j(2\pi f/c)r_{m,n}}}{4\pi r_{m,n}}. \tag{4.4}$$

The nth column of the matrix $\mathbf{A}^{(f)}$, $\mathbf{a}_n^{(f)}$, is the replica vector, which reflects the transmission from the nth potential noise source to the hydrophones.

For localizing the multi-frequency sources, we can extend the normalized version of the sparse measurement model, $\tilde{\mathbf{t}}^{(f)} = \tilde{\mathbf{A}}^{(f)}\tilde{\mathbf{w}}^{(f)}$, as a block-sparse measurement model with L frequencies $(f_1, \cdots, f_L)$

$$\tilde{\mathbf{t}} = \tilde{\mathbf{A}}\tilde{\mathbf{w}} + \tilde{\mathbf{n}}, \tag{4.5}$$

where multiple-frequency measurement vector $\tilde{\mathbf{y}} \in \mathbb{C}^{ML}$, sensing matrix of block-sparse model $\tilde{\mathbf{A}} \in \mathbb{C}^{ML\times NL}$ (M: number of receivers, N: number of potential sources, L: number of frequencies). Multiple-frequency measurement vector $\tilde{\mathbf{t}}$ and block-sparse vector $\tilde{\mathbf{w}} \in \mathbb{C}^{NL}$ take the forms,

$$\begin{aligned}\tilde{\mathbf{t}} &= [\tilde{\mathbf{t}}_1^{\text{block}}; \cdots ; \tilde{\mathbf{t}}_M^{\text{block}}] \\ &= [\underbrace{\tilde{t}_1^{(f_1)}, \cdots, \tilde{t}_1^{(f_L)}}_{\tilde{\mathbf{t}}_1^{\text{block}}}, \cdots, \underbrace{\tilde{t}_M^{(f_1)}, \cdots, \tilde{t}_M^{(f_L)}}_{\tilde{\mathbf{t}}_M^{\text{block}}}]^{\mathsf{T}},\end{aligned} \tag{4.6}$$

$$\begin{aligned}\tilde{\mathbf{w}} &= [\tilde{\mathbf{w}}_1^{\text{block}}; \cdots ; \tilde{\mathbf{w}}_N^{\text{block}}] \\ &= [\underbrace{\tilde{w}_1^{(f_1)}, \cdots, \tilde{w}_1^{(f_L)}}_{\tilde{\mathbf{x}}_1^{\text{block}}}, \cdots, \underbrace{\tilde{w}_N^{(f_1)}, \cdots, \tilde{x}_N^{(f_L)}}_{\tilde{\mathbf{x}}_N^{\text{block}}}]^{\mathsf{T}},\end{aligned} \tag{4.7}$$

and

$$\tilde{\mathbf{A}} = \begin{bmatrix} \tilde{\mathbf{A}}_{1,1}^{\text{block}} & \cdots & \tilde{\mathbf{A}}_{1,N}^{\text{block}} \\ \vdots & \ddots & \vdots \\ \tilde{\mathbf{A}}_{M,1}^{\text{block}} & \cdots & \tilde{\mathbf{A}}_{M,N}^{\text{block}} \end{bmatrix}, \tag{4.8}$$

where $\tilde{\mathbf{A}}_{m,n}^{\text{block}}$ is the (m,n)th partition of the matrix $\tilde{\mathbf{A}}$,

$$\begin{aligned} \tilde{\mathbf{A}}_{m,n}^{\text{block}} &= \text{diag}\left(\hat{a}_{m,n}^{(f_1)}, \cdots, \hat{a}_{m,n}^{(f_L)}\right) \\ &= \begin{bmatrix} \hat{a}_{m,n}^{(f_1)} & 0 & \cdots & 0 \\ 0 & \hat{a}_{m,n}^{(f_2)} & \cdots & 0 \\ \vdots & \vdots & \ddots & \vdots \\ 0 & 0 & \cdots & \hat{a}_{m,n}^{(f_L)} \end{bmatrix}, \end{aligned} \tag{4.9}$$

and $\hat{a}_{m,n}^{(f_l)}$ is the (m,n)th entry of the matrix $\tilde{\mathbf{A}}^{(f_l)}$. Note that the solution $\tilde{\mathbf{x}}$ is blockwise sparse. Readers are referred to Sec.3.2.3. for detailed description.

4.2.2 Coherent multiple-frequency localization with block-sparse Bayesian learning technique

To estimate the broadband source locations, we adopted the block-sparse Bayesian learning(BSBL) method. In the BSBL framework, the amplitudes of each potential noise source $\tilde{\mathbf{w}}_i \in \mathbb{C}^L$ are assumed as parameterized multivariated Gaussian distribution.

$$p(\tilde{\mathbf{w}}_i; \gamma_i, \mathbf{B}_i) \sim \mathcal{N}(0, \gamma_i \mathbf{B}_i), \quad i = 1, \cdots, N \tag{4.10}$$

where γ_i is a hyperparameter controlling the block-sparsity and $\mathbf{B}_i \in \mathbb{R}^{L \times L}$ is a intra-block correlation matrix which captures the correlation structure of the i-th block.

Under the assumption that the prior of $\tilde{\mathbf{w}}$ satisfies $p(\tilde{\mathbf{w}}; \{\gamma_i, \mathbf{B}_i\}_i)) \sim \mathcal{N}(0, \boldsymbol{\Sigma}_0)$ and noise vector satisfies $p(\tilde{\mathbf{n}}; \lambda) \sim \mathcal{N}(0, \sigma^2\mathbf{I})$, the the posterior of $\tilde{\mathbf{w}}$ can be described as,

$$p(\tilde{\mathbf{w}}|\tilde{\mathbf{t}}; \{\gamma_i, \mathbf{B}_i\}_{i=1}^N) = \mathcal{N}(\boldsymbol{\mu}_{\tilde{w}}, \boldsymbol{\Sigma}_{\tilde{w}}) \tag{4.11}$$

where $\boldsymbol{\Sigma}_0$ is a covariance matrix of system ($\boldsymbol{\Sigma}_0 = \text{diag}\{\gamma_1\mathbf{B}_1, \cdots, \gamma_N\mathbf{B}_N\}$) and σ^2 is a noise variance. Then below stochastic model can be adopted to solve the spectrally joint sparse problem.

$$\boldsymbol{\mu}_{\tilde{w}} = \boldsymbol{\Sigma}_0\tilde{\mathbf{A}}^H\big(\sigma^2\mathbf{I} + \tilde{\mathbf{A}}\boldsymbol{\Sigma}_0\tilde{\mathbf{A}}^H\big)^{-1}\tilde{\mathbf{t}}, \tag{4.12}$$

$$\boldsymbol{\Sigma}_{\tilde{w}} = \big({\boldsymbol{\Sigma}_0}^{-1} + \frac{1}{\sigma^2}\tilde{\mathbf{A}}^H\tilde{\mathbf{A}}\big)^{-1} + \tilde{\mathbf{t}} \tag{4.13}$$

Then, the parameters can be estimated by using the Type-II maximum likelihood procedure. This is equivalent to minimizing the following equation,

$$\log|\sigma^2\mathbf{I} + \tilde{\mathbf{A}}\boldsymbol{\Sigma}_0\tilde{\mathbf{A}}^H| + \tilde{\mathbf{t}}^H\big(\sigma^2\mathbf{I} + \tilde{\mathbf{A}}\boldsymbol{\Sigma}_0\tilde{\mathbf{A}}^H\big)^{-1}\tilde{\mathbf{t}} \tag{4.14}$$

And the following Expectation Maximization method(EM-method) can be applied to learning the γ_i, σ^2 and $\mathbf{B}_i$.

$$\gamma_i = \frac{1}{L}\text{Tr}\big[{\mathbf{B}_i}^{-1}\big(\boldsymbol{\Sigma}_{\tilde{w}}^i + \mu_{\tilde{w}}^i{\mu_{\tilde{w}}^i}^H\big)\big] \tag{4.15}$$

$$\sigma^2 = \frac{||\tilde{\mathbf{t}} - \tilde{\mathbf{A}}\boldsymbol{\mu}_{\tilde{w}}||_2^2 + \text{Tr}(\boldsymbol{\Sigma}_{\tilde{w}}\tilde{\mathbf{A}}^H\tilde{\mathbf{A}})}{M} \tag{4.16}$$

$$\mathbf{B}_i = \mathbf{B}(\forall i) = \frac{1}{N}\sum_{i=1}^{N}\frac{\boldsymbol{\Sigma}_{\tilde{w}}^i + \mu_{\tilde{w}}^i \mu_{\tilde{w}}^{i\ H}}{\gamma_i} \tag{4.17}$$

After a few iterations, we can finally obtain the sparse amplitudes of potential noise sources as $\tilde{\mathbf{w}} \approx \boldsymbol{\mu}_{\tilde{w}}$.

4.2.3 3-dimensional off grid source localization method

In the 3-dimensional source localization problem, estimating the basis mismatch error is a trivial problem since the following reasons.

1. Considering the spherical spreading noise source, first-order approximation of the transfer function is not available.

2. To estimate the basis mismatch error, the three-axis components of the basis mismatch error should be jointly considered.

In the traditional OGSBI framework, there is no way to solve these problems since basis mismatch error could not be linearized with the fixed basis. Instead, we introduce a basis that varies with each iteration. If the basis represents the exact source locations, there is no need to consider the basis mismatch error. In this chapter, we will show how the proposed basis, namely "flexible grid points", could reduce the basis mismatch error.

To treat the basis mismatch error, we formulated the new relationship between the measurement vector and the solution vector as below.

$$\tilde{\mathbf{t}} = \big(\tilde{\mathbf{A}} + \tilde{\mathbf{D}}_x\text{diag}(\Delta\mathbf{x}) + \tilde{\mathbf{D}}_y\text{diag}(\Delta\mathbf{y}) + \tilde{\mathbf{D}}_z\text{diag}(\Delta\mathbf{z})\big)\tilde{\mathbf{w}} + \tilde{\mathbf{n}}, \tag{4.18}$$

where $\boldsymbol{\Delta}\mathbf{x}, \boldsymbol{\Delta}\mathbf{y}, \boldsymbol{\Delta}\mathbf{z}$ are the directional basis mismatch error vector and $\tilde{\mathbf{D}}_x, \tilde{\mathbf{D}}_y, \tilde{\mathbf{D}}_z$ are the directional first order derivative of $\tilde{\mathbf{A}}$ corresponding to each potential source locations.

$$\tilde{\mathbf{D}}_{\mathbf{x}} = \frac{\partial}{\partial x}\begin{bmatrix} \tilde{\mathbf{A}}^{\text{block}}_{1,1} & \cdots & \tilde{\mathbf{A}}^{\text{block}}_{1,N} \\ \vdots & \ddots & \vdots \\ \tilde{\mathbf{A}}^{\text{block}}_{M,1} & \cdots & \tilde{\mathbf{A}}^{\text{block}}_{M,N} \end{bmatrix}$$

$$\tilde{\mathbf{D}}_{\mathbf{y}} = \frac{\partial}{\partial y}\begin{bmatrix} \tilde{\mathbf{A}}^{\text{block}}_{1,1} & \cdots & \tilde{\mathbf{A}}^{\text{block}}_{1,N} \\ \vdots & \ddots & \vdots \\ \tilde{\mathbf{A}}^{\text{block}}_{M,1} & \cdots & \tilde{\mathbf{A}}^{\text{block}}_{M,N} \end{bmatrix} \tag{4.19}$$

$$\tilde{\mathbf{D}}_{\mathbf{z}} = \frac{\partial}{\partial z}\begin{bmatrix} \tilde{\mathbf{A}}^{\text{block}}_{1,1} & \cdots & \tilde{\mathbf{A}}^{\text{block}}_{1,N} \\ \vdots & \ddots & \vdots \\ \tilde{\mathbf{A}}^{\text{block}}_{M,1} & \cdots & \tilde{\mathbf{A}}^{\text{block}}_{M,N} \end{bmatrix}$$

$$
\begin{aligned}
\Delta\mathbf{x} &= [\Delta\mathbf{x}_1^{\text{block}}; \cdots ; \Delta\mathbf{x}_N^{\text{block}}] \\
&= [\underbrace{\Delta x_1^{(f_1)}, \cdots, \Delta x_1^{(f_L)}}_{\Delta\mathbf{x}_1^{\text{block}}}, \cdots, \underbrace{\Delta x_N^{(f_1)}, \cdots, \Delta x_N^{(f_L)}}_{\Delta\mathbf{x}_N^{\text{block}}}]^{\mathsf{T}} \\
\Delta\mathbf{y} &= [\Delta\mathbf{y}_1^{\text{block}}; \cdots ; \Delta\mathbf{y}_N^{\text{block}}] \\
&= [\underbrace{\Delta y_1^{(f_1)}, \cdots, \Delta y_1^{(f_L)}}_{\Delta\mathbf{y}_1^{\text{block}}}, \cdots, \underbrace{\Delta y_N^{(f_1)}, \cdots, \Delta y_N^{(f_L)}}_{\Delta\mathbf{y}_N^{\text{block}}}]^{\mathsf{T}} \\
\Delta\mathbf{z} &= [\Delta\mathbf{z}_1^{\text{block}}; \cdots ; \Delta\mathbf{z}_N^{\text{block}}] \\
&= [\underbrace{\Delta z_1^{(f_1)}, \cdots, \Delta z_1^{(f_L)}}_{\Delta\mathbf{z}_1^{\text{block}}}, \cdots, \underbrace{\Delta z_N^{(f_1)}, \cdots, \Delta z_N^{(f_L)}}_{\Delta\mathbf{z}_N^{\text{block}}}]^{\mathsf{T}}
\end{aligned}
\tag{4.20}
$$

Note that each directional basis mismatch value is equivalent when they are located in the same ith block($e.g.$, the elements of $\Delta\mathbf{x}_i^{(f_j)}$ are all equivalent for $\forall j$). Thus, directional basis mismatch error vectors can be described as below.

$$
\begin{aligned}
\tilde{\mathbf{t}} &= \left(\tilde{\mathbf{A}} + \tilde{\mathbf{D}}_x\Delta\mathbf{X} + \tilde{\mathbf{D}}_y\Delta\mathbf{Y} + \tilde{\mathbf{D}}_z\Delta\mathbf{Z}\right)\tilde{\mathbf{w}} + \tilde{\mathbf{n}} \\
&= \mathbf{\Phi}\tilde{\mathbf{w}} + \tilde{\mathbf{n}}
\end{aligned}
\tag{4.21}
$$

where $\mathbf{\Phi}$ is the newly updated basis and $\Delta\mathbf{X}, \Delta\mathbf{Y}, \Delta\mathbf{Z}$ are the block diagonal matrix with,

$$
\mathbf{\Phi} = \tilde{\mathbf{A}} + \tilde{\mathbf{D}}_x\Delta\mathbf{X} + \tilde{\mathbf{D}}_y\Delta\mathbf{Y} + \tilde{\mathbf{D}}_z\Delta\mathbf{Z} \tag{4.22}
$$

$$
\begin{aligned}
\Delta\mathbf{X} &= \text{diag}(\Delta x_1\mathbf{I}_L, \cdots, \Delta x_N\mathbf{I}_L) \\
\Delta\mathbf{Y} &= \text{diag}(\Delta y_1\mathbf{I}_L, \cdots, \Delta y_N\mathbf{I}_L) \\
\Delta\mathbf{Z} &= \text{diag}(\Delta z_1\mathbf{I}_L, \cdots, \Delta z_N\mathbf{I}_L)
\end{aligned}
\tag{4.23}
$$

This model presents a new approach which can reduce the basis mismatch error in 3-dimensional localization problem.

1. Inference of basis : If all sparse sources are lie on the basis Φ, directional basis mismatch error matrix $\Delta\mathbf{X}, \Delta\mathbf{Y}, \Delta\mathbf{Z}$ should be zero. Thus, we seeks for the basis with $\Delta\mathbf{X} = \Delta\mathbf{Y} = \Delta\mathbf{Z} = 0$

2. Inference of parameters : There are 6 unknown parameters $\boldsymbol{\gamma}, \mathbf{B}, \sigma^2, \Delta\mathbf{x}, \Delta\mathbf{y}, \Delta\mathbf{z}$. In the EM approach, we can obtain the all unknown parameters by using a Type II maximum likelihood procedure.

Then the BSBL-based approach in Sec.4.2.2 can be utilized to estimate the unknown parameters. The stochastic model is exactly the same as on grid BSBL model as below.

$$\log|\sigma^2\mathbf{I} + \boldsymbol{\Phi}\boldsymbol{\Sigma}_0\boldsymbol{\Phi}^H| + \tilde{\mathbf{t}}^H\left(\sigma^2\mathbf{I} + \boldsymbol{\Phi}\boldsymbol{\Sigma}_0\boldsymbol{\Phi}^H\right)^{-1}\tilde{\mathbf{t}} \tag{4.24}$$

Note that the basis matrix $\boldsymbol{\Phi}$ is treated as a variable in this case. Then the Expectation Maximization method(EM-method) can be applied to learning the γ_i, σ^2 and $\mathbf{B}_i$.

$$\gamma_i = \frac{1}{L}\mathrm{Tr}\left[{\mathbf{B}_i}^{-1}\left(\boldsymbol{\Sigma}_{\tilde{w}}^i + \mu_{\tilde{w}}^i {\mu_{\tilde{w}}^i}^H\right)\right] \tag{4.25}$$

$$\sigma^2 = \frac{||\tilde{\mathbf{t}} - \boldsymbol{\Phi}\boldsymbol{\mu}_{\tilde{w}}||_2^2 + \mathrm{Tr}(\boldsymbol{\Sigma}_{\tilde{w}}\boldsymbol{\Phi}^H\boldsymbol{\Phi})}{M} \tag{4.26}$$

$$\mathbf{B}_i = \mathbf{B}(\forall i) = \frac{1}{N}\sum_{i=1}^{N}\frac{\boldsymbol{\Sigma}_{\tilde{w}}^i + \mu_{\tilde{w}}^i {\mu_{\tilde{w}}^i}^H}{\gamma_i} \tag{4.27}$$

For the estimation of the basis mismatch error $\Delta\mathbf{x}, \Delta\mathbf{y}, \Delta\mathbf{z}$, we should maximize the following expectation,

$$\begin{aligned}&\mathbf{E}\{\log p(\tilde{\mathbf{t}}|\tilde{\mathbf{w}}, \sigma^2, \Delta\mathbf{x}, \Delta\mathbf{y}, \Delta\mathbf{z})\}\\&= \mathbf{E}\{||\tilde{\mathbf{t}} - (\tilde{\mathbf{A}} + \tilde{\mathbf{D}}_x\Delta\mathbf{X} + \tilde{\mathbf{D}}_y\Delta\mathbf{Y} + \tilde{\mathbf{D}}_z\Delta\mathbf{Z})\tilde{\mathbf{w}}||_2^2\}\end{aligned} \tag{4.28}$$

This equation is equivalent to the following equation.

$$\begin{aligned}&\mathbf{E}\{||\tilde{\mathbf{t}} - (\tilde{\mathbf{A}} + \tilde{\mathbf{D}}_x\Delta\mathbf{X} + \tilde{\mathbf{D}}_y\Delta\mathbf{Y} + \tilde{\mathbf{D}}_z\Delta\mathbf{Z})\tilde{\mathbf{w}}||_2^2\}\\&= ||\tilde{\mathbf{t}} - (\tilde{\mathbf{A}} + \tilde{\mathbf{D}}_x\Delta\mathbf{X} + \tilde{\mathbf{D}}_y\Delta\mathbf{Y} + \tilde{\mathbf{D}}_z\Delta\mathbf{Z})\boldsymbol{\mu}_{\tilde{w}}\}||_2^2\\&+ \sum_{i=1}^{N} \mathrm{Tr}\Big[\boldsymbol{\Sigma}_{\tilde{w},i}(\tilde{\mathbf{A}}_i + \tilde{\mathbf{D}}_{x,i}\Delta\mathbf{X}_i)^H(\tilde{\mathbf{A}}_i + \tilde{\mathbf{D}}_{x,i}\Delta\mathbf{X}_i)\Big]\\&+ \sum_{i=1}^{N} \mathrm{Tr}\Big[\boldsymbol{\Sigma}_{\tilde{w},i}(\tilde{\mathbf{A}}_i + \tilde{\mathbf{D}}_{y,i}\Delta\mathbf{Y}_i)^H(\tilde{\mathbf{A}}_i + \tilde{\mathbf{D}}_{y,i}\Delta\mathbf{Y}_i)\Big]\\&+ \sum_{i=1}^{N} \mathrm{Tr}\Big[\boldsymbol{\Sigma}_{\tilde{w},i}(\tilde{\mathbf{A}}_i + \tilde{\mathbf{D}}_{z,i}\Delta\mathbf{Z}_i)^H(\tilde{\mathbf{A}}_i + \tilde{\mathbf{D}}_{z,i}\Delta\mathbf{Z}_i)\Big]\end{aligned} \tag{4.29}$$

where $[\tilde{\mathbf{A}}_i, \tilde{\mathbf{D}}_{x,i}, \tilde{\mathbf{D}}_{y,i}, \tilde{\mathbf{D}}_{z,i}]$ are the i-th blocks of $[\tilde{\mathbf{A}}, \tilde{\mathbf{D}}_x, \tilde{\mathbf{D}}_y, \tilde{\mathbf{D}}_z]$ and $[\boldsymbol{\Sigma}_{\tilde{w},i}, \Delta\mathbf{X}_i, \Delta\mathbf{Y}_i, \Delta\mathbf{Z}_i]$ are the i-th diagonal blocks of $[\boldsymbol{\Sigma}_{\tilde{w}}, \Delta\mathbf{X}, \Delta\mathbf{Y}, \Delta\mathbf{Z}]$. This equation can be simply summarized by,

$$\begin{aligned}&\mathbf{E}\{\log p(\tilde{\mathbf{t}}|\tilde{\mathbf{w}}, \sigma^2, \Delta\mathbf{x}, \Delta\mathbf{y}, \Delta\mathbf{z})\}\\&= \Delta\boldsymbol{x}^T(\mathbf{Q}_{x,1} + \mathbf{Q}_{x,2})\Delta\boldsymbol{x} - 2(\mathbf{R}_{x,1} + \mathbf{R}_{x,2})\Delta\boldsymbol{x} + C_x\\&+ \Delta\boldsymbol{y}^T(\mathbf{Q}_{y,1} + \mathbf{Q}_{y,2})\Delta\boldsymbol{y} - 2(\mathbf{R}_{y,1} + \mathbf{R}_{y,2})\Delta\boldsymbol{y} + C_y\\&+ \Delta\boldsymbol{z}^T(\mathbf{Q}_{z,1} + \mathbf{Q}_{z,2})\Delta\boldsymbol{z} - 2(\mathbf{R}_{z,1} + \mathbf{R}_{z,2})\Delta\boldsymbol{z} + C_z\end{aligned} \tag{4.30}$$

where,

$$
\begin{aligned}
\mathbf{Q}_{x,1} &= \sum_{j=1}^{L} (\overline{\tilde{\mathbf{D}}_{x,f_j}^{H} \tilde{\mathbf{D}}_{x,f_j}}) \odot \boldsymbol{\mu}_{\tilde{w},f_j} \boldsymbol{\mu}_{\tilde{w},f_j}{}^{H}) \\
\mathbf{Q}_{y,1} &= \sum_{j=1}^{L} (\overline{\tilde{\mathbf{D}}_{y,f_j}^{H} \tilde{\mathbf{D}}_{y,f_j}}) \odot \boldsymbol{\mu}_{\tilde{w},f_j} \boldsymbol{\mu}_{\tilde{w},f_j}{}^{H}) \\
\mathbf{Q}_{z,1} &= \sum_{j=1}^{L} (\overline{\tilde{\mathbf{D}}_{z,f_j}^{H} \tilde{\mathbf{D}}_{z,f_j}}) \odot \boldsymbol{\mu}_{\tilde{w},f_j} \boldsymbol{\mu}_{\tilde{w},f_j}{}^{H}) \\
\mathbf{R}_{x,1} &= \mathrm{Re}\Big[\sum_{j=1}^{L} \mathrm{diag}(\boldsymbol{\mu}_{\tilde{w},f_j}) \tilde{\boldsymbol{D}}_{x,f_j}^{H} (\mathbf{t}_{f_j} - \tilde{\mathbf{A}} \boldsymbol{\mu}_{\tilde{w},f_j}) \Big]^{T} \Delta \boldsymbol{x} \\
\mathbf{R}_{y,1} &= \mathrm{Re}\Big[\sum_{j=1}^{L} \mathrm{diag}(\boldsymbol{\mu}_{\tilde{w},f_j}) \tilde{\boldsymbol{D}}_{y,f_j}^{H} (\mathbf{t}_{f_j} - \tilde{\mathbf{A}} \boldsymbol{\mu}_{\tilde{w},f_j}) \Big]^{T} \Delta \boldsymbol{y} \\
\mathbf{R}_{z,1} &= \mathrm{Re}\Big[\sum_{j=1}^{L} \mathrm{diag}(\boldsymbol{\mu}_{\tilde{w},f_j}) \tilde{\boldsymbol{D}}_{z,f_j}^{H} (\mathbf{t}_{f_j} - \tilde{\mathbf{A}} \boldsymbol{\mu}_{\tilde{w},f_j}) \Big]^{T} \Delta \boldsymbol{z}
\end{aligned}
\tag{4.31}
$$

And $[\mathbf{Q}_{x,2}, \mathbf{Q}_{y,2}, \mathbf{Q}_{z,2}, \mathbf{R}_{x,2}, \mathbf{R}_{y,2}, \mathbf{R}_{z,2}]$ are the diagonal matrices and (i,i)th element of each matrix can be described as below

$$
\begin{aligned}
\mathbf{Q}_{x,2}^{(i,i)} &= \mathrm{Tr}(\boldsymbol{\Sigma}_{\tilde{w},i} \tilde{\mathbf{D}}_{x,i}^{H} \tilde{\mathbf{D}}_{x,i}) \\
\mathbf{Q}_{y,2}^{(i,i)} &= \mathrm{Tr}(\boldsymbol{\Sigma}_{\tilde{w},i} \tilde{\mathbf{D}}_{y,i}^{H} \tilde{\mathbf{D}}_{y,i}) \\
\mathbf{Q}_{z,2}^{(i,i)} &= \mathrm{Tr}(\boldsymbol{\Sigma}_{\tilde{w},i} \tilde{\mathbf{D}}_{z,i}^{H} \tilde{\mathbf{D}}_{z,i}) \\
\mathbf{R}_{x,2}^{(i,i)} &= \mathrm{Tr}(2\boldsymbol{\Sigma}_{x,i} \,\mathrm{Re}(\tilde{\mathbf{A}}_{i}^{H} \tilde{\mathbf{D}}_{x,i})) \\
\mathbf{R}_{y,2}^{(i,i)} &= \mathrm{Tr}(2\boldsymbol{\Sigma}_{y,i} \,\mathrm{Re}(\tilde{\mathbf{A}}_{i}^{H} \tilde{\mathbf{D}}_{y,i})) \\
\mathbf{R}_{z,2}^{(i,i)} &= \mathrm{Tr}(2\boldsymbol{\Sigma}_{z,i} \,\mathrm{Re}(\tilde{\mathbf{A}}_{i}^{H} \tilde{\mathbf{D}}_{z,i}))
\end{aligned}
\tag{4.32}
$$

Then, the directional basis mismatch values which maximize the expectation should satisfy following equations.

$$\begin{aligned}
\frac{\partial}{\partial x}\left[\boldsymbol{\Delta x}^T(\mathbf{Q}_{x,1}+\mathbf{Q}_{x,2})\boldsymbol{\Delta x}-2(\mathbf{R}_{x,1}+\mathbf{R}_{x,2})\boldsymbol{\Delta x}+C_x\right]&=0\\
\frac{\partial}{\partial y}\left[\boldsymbol{\Delta y}^T(\mathbf{Q}_{y,1}+\mathbf{Q}_{y,2})\boldsymbol{\Delta y}-2(\mathbf{R}_{y,1}+\mathbf{R}_{y,2})\boldsymbol{\Delta y}+C_y\right]&=0\\
\frac{\partial}{\partial z}\left[\boldsymbol{\Delta z}^T(\mathbf{Q}_{z,1}+\mathbf{Q}_{z,2})\boldsymbol{\Delta x}-2(\mathbf{R}_{z,1}+\mathbf{R}_{z,2})\boldsymbol{\Delta z}+C_z\right]&=0
\end{aligned} \tag{4.33}$$

Thus, the directional basis mismatch errors could be obtained as follow.

$$\begin{aligned}
\boldsymbol{\Delta x}&=(\mathbf{Q}_{x,1}+\mathbf{Q}_{x,2})^{-1}(\mathbf{R}_{x,1}+\mathbf{R}_{x,2})\\
\boldsymbol{\Delta y}&=(\mathbf{Q}_{y,1}+\mathbf{Q}_{y,2})^{-1}(\mathbf{R}_{y,1}+\mathbf{R}_{y,2})\\
\boldsymbol{\Delta z}&=(\mathbf{Q}_{z,1}+\mathbf{Q}_{z,2})^{-1}(\mathbf{R}_{z,1}+\mathbf{R}_{z,2})
\end{aligned} \tag{4.34}$$

Note that these estimated values just provide us whether the present grid points have a basis mismatch errors or not since the linear approximation of 3-dimensional grid points is not available. Thus, we have to update the basis according to these estimated values until $\Delta\boldsymbol{x}, \Delta\boldsymbol{y}, \Delta\boldsymbol{z}$ going to be zero. By using the estimated values, we update the following matrices.

$$
\begin{aligned}
\mathbf{\Phi}^{(new)} &\leftarrow \tilde{\mathbf{A}}^{(old)} + \tilde{\mathbf{D}}_x^{(old)}\Delta\mathbf{X} + \tilde{\mathbf{D}}_y^{(old)}\Delta\mathbf{Y} + \tilde{\mathbf{D}}_z^{(old)}\Delta\mathbf{Z} \\
\tilde{\mathbf{A}}^{(new)} &\leftarrow \mathbf{\Phi}^{(old)} \\
\tilde{\mathbf{D}}_{\mathbf{x}}^{(new)} &\leftarrow \frac{\partial}{\partial x}\tilde{\mathbf{A}}^{(new)} \\
\tilde{\mathbf{D}}_{\mathbf{y}}^{(new)} &\leftarrow \frac{\partial}{\partial y}\tilde{\mathbf{A}}^{(new)} \\
\tilde{\mathbf{D}}_{\mathbf{z}}^{(new)} &\leftarrow \frac{\partial}{\partial z}\tilde{\mathbf{A}}^{(new)}
\end{aligned}
\tag{4.35}
$$

4.3 Simulation and Experiment Results

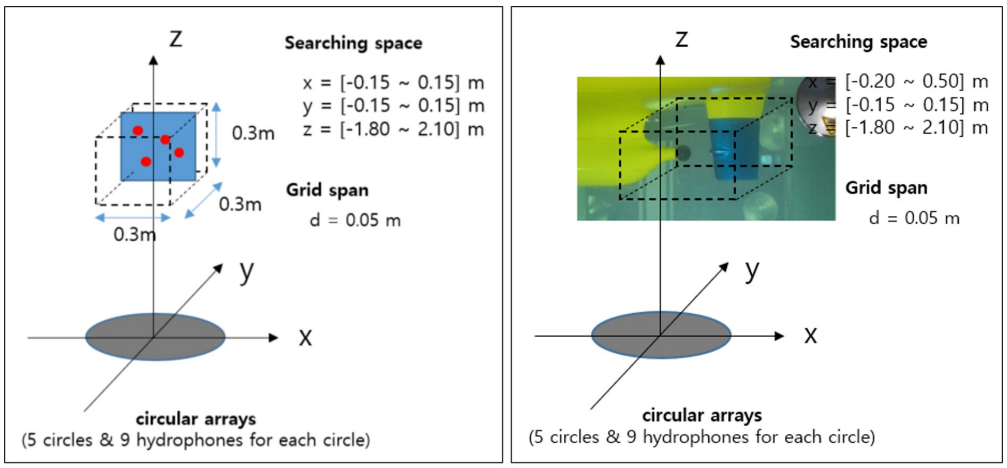

Figure 4.1: (a) Simulation Condition for 4 monopole type source localization with basis mismatch (b) Transducer source experiment setup

To validate the proposed methods, the localizations with simulated and experimental data were conducted. Fig.4.1.(a) shows the simulated data which have 4 monopole type sources and Fig.4.1.(b) shows the experimental data which have 1 monopole type source. For the localization, 21 frequency components and 45 hydrophones were used and grid points were uniformly distributed with 0.05m grid span.

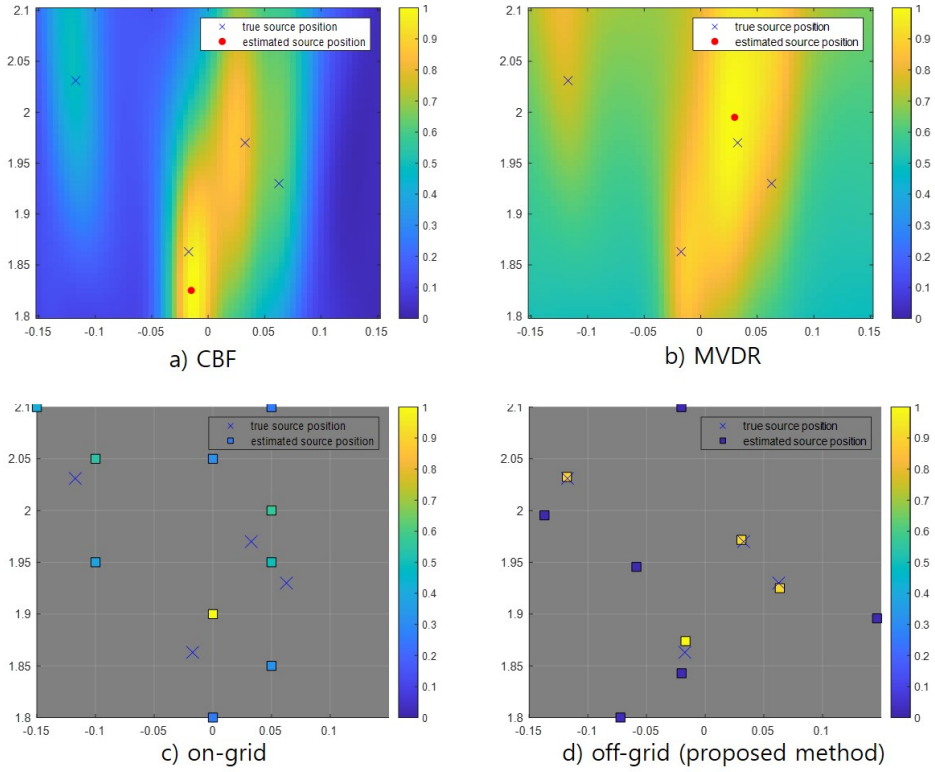

Figure 4.2: Simulated data localization results (a) CBF (b) MVDR (c) Conventional CS-based method (d) Proposed method

Fig.4.2. shows the localization results with simulated data. The traditional beamforming processors(Fig.4.2.(a) and Fig.4.2.(b)) only show the ambiguous results. Conventional CS-based method(Fig.4.2.(c)) shows the sparse source locations, however, localization accuracy is poor since the method could not reduce the basis mismatch error. In other hand, the proposed method(Fig.4.2.(d)) reveals the exact source positions.

Fig.4.3. shows the localization result of broadband transmitter. By reducing the basis mismatch, the result of the proposed method indicates one sparse source position(Fig.4.3.(a)). However, Conventional CS-based method(Fig.4.3.(b)) does not seek a sparse solution.

Moreover, source localization using the real cavitation experiment data is con-

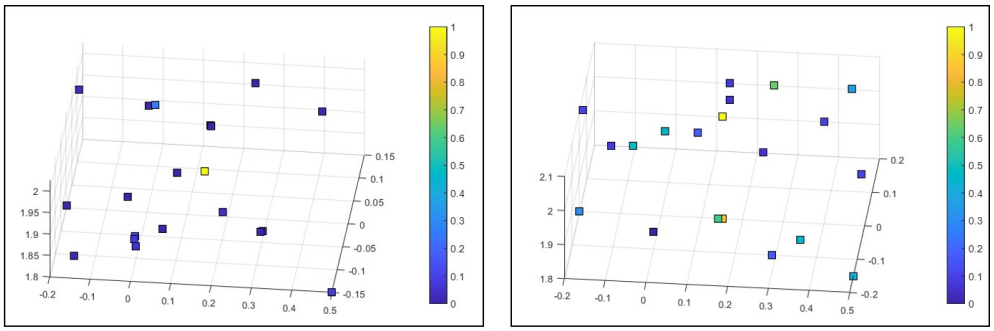

Figure 4.3: Transducer source localization results (a) Proposed method (b) Conventional CS method

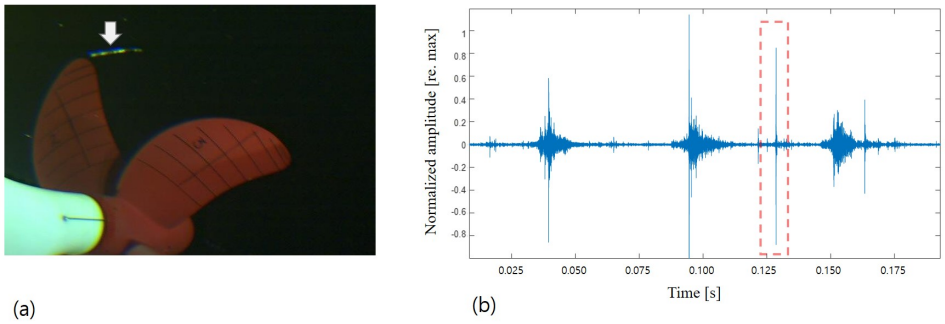

Figure 4.4: (a) TVC visual observation (b) Pop type TVC signal

ducted. As shown in FIg.4.4., we used pop type cavitation signal data to validate the proposed method in this localization procedure. FIg.4.5. shows the localization results using the traditional beamforming processor(CBF). FIg.4.6. shows the localization results using the proposed off grid method. It is shown that the estimated source location is not lied on the initial grid points. This means that the proposed method can localize the noise source considering the basis mismatch error.

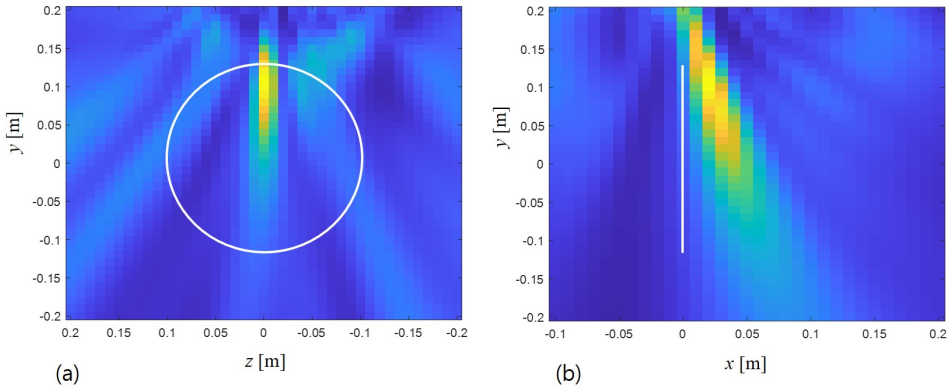

Figure 4.5: Localization results of Conventional Beamforming

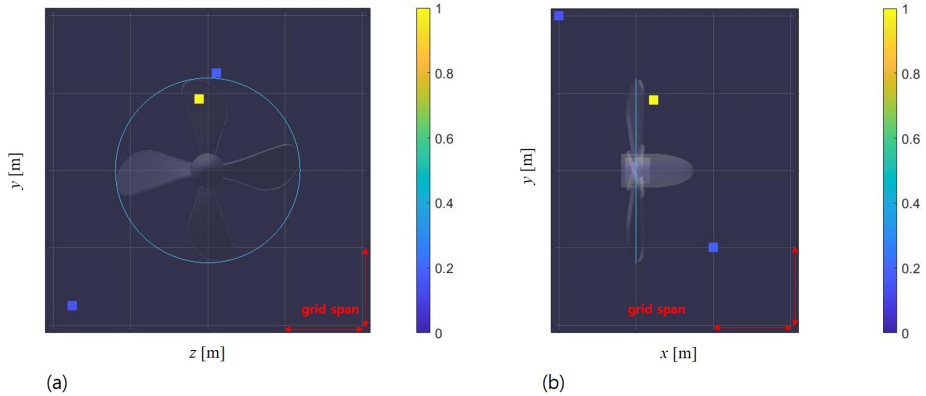

Figure 4.6: Localization results of proposed method

4.4 Conclusion

The purpose of this chapter is to localize the broadband noise source accurately by reducing the basis mismatch error. To estimate the exact basis mismatch error, the coherent multiple-frequency processing and the OGSBI based approach are proposed. In contrast to the coherent multiple-frequency processing, the proposed method provides accurate localization results regardless of basis mismatch issue. However, it was shown that the proposed method is not robust to noise compared to conventional CS-

Table 4.1: Summary of the proposed method

3D off-grid source localization method	
Methodologies	• Block-spare Bayesian learning(BSBL) • Stochastic model (Type-II maximum likelihood procedure) • Adopting the coherent multiple-frequency processing
Advantages	• Reduce the modeling error induced by basis mismatch • Computational efficiency
Limitations	• Degraded performance under heavy background noise

based methods. In this work, off grid technique which is applicable to 3D source localization problem is firstly presented and the technique is validated with simulation and experiment results.

References

[1]N. A. Chang and D. R. Dowling, “Ray-based acoustic localization of cavitation in a highly reverberant environment”, J. Acoust. Soc. Am. **125**, 3088–3100 (2009).

[2]N. A. Chang and S. L. Ceccio, “The acoustic emissions of cavitation bubbles in stretched vortices”, J. Acoust. Soc. Am. **130**, 3209–3219 (2011).

[3]C. Park, H. Seol, K. Kim, and W. Seong, “A study on propeller noise source localization in a cavitation tunnel”, Ocean Eng. **36**, 754–762 (2009).

[4]D. Kim, W. Seong, Y. Choo, and J. Lee, “Localization of incipient tip vortex cavitation using ray based matched field inversion method”, J. Sound Vib. **354**, 34–46 (2015).

[5]K. Lee, J. Lee, D. Kim, K. Kim, and W. Seong, “Propeller sheet cavitation noise source modeling and inversion”, J. Sound Vib. **333**, 1356–1368 (2014).

[6]D. Kim, K. Lee, and W. Seong, “Non-cavitating propeller noise modeling and inversion”, J. Sound Vib. **333**, 6424–6437 (2014).

[7]C. Park, G. Kim, Y. Park, K. Lee, and W. Seong, “Noise localization method for model tests in a large cavitation tunnel using a hydrophone array”, Remote Sens. **8**, 195 (2016).

[8]D. L. Donoho, “Compressed sensing”, IEEE Trans. Inf. Theory **52**, 1289–1306 (2006).

[9]D. Malioutov, M. Cetin, and A. Willsky, “A sparse signal reconstruction perspective for source localization with sensor arrays”, IEEE Trans. Signal Process. **53**, 3010–3022 (2005).

[10]A. Xenakia and P. Gerstoft, “Compressive beamforming”, J. Acoust. Soc. Am. **136**, 260–271 (2014).

[11]C. Yardim, P. Gerstoft, W. S. Hodgkiss, and J. Traer, “Compressive geoacoustic inversion using ambient noise”, J. Acoust. Soc. Am. **135**, 1245–1255 (2014).

[12]P. A. Forero and P. A. Baxley, “Shallow-water sparsity-cognizant source-location mapping”, J. Acoust. Soc. Am. **135**, 3483–3501 (2014).

[13]G. Chardon, L. Daudet, A. Peillot, F. Ollivier, N. Bertin, and R. Gribonval, “Near-field acoustic holography using sparse regularization and compressive sampling principles”, J. Acoust. Soc. Am. **132**, 1521–1534 (2012).

[14]E. Fernandez-Grande, A. Xenaki, and P. Gerstoft, “A sparse equivalent source method for near-field acoustic holography”, J. Acoust. Soc. Am. **141**, 532–542 (2017).

[15]N. Wagner, Y. C. Eldar, and Z. Friedman, “Compressed beamforming in ultrasound imaging”, IEEE Trans. Signal Process. **60**, 4643–4657 (2012).

[16]Y. Choo and W. Seong, “Compressive spherical beamforming for localization of incipient tip vortex cavitation”, J. Acoust. Soc. Am. **140**, 4085–4090 (2016).

[17]M. Park, Y. Park, K. Lee, and W. Seong, “Incipient tip vortex cavitation localization using block-sparse compressive sensing”, J. Acoust. Soc. Am. **147**, 3454–3464 (2016).

[18]M. E. Tipping, “Sparse bayesian learning and the relevance vector machine”, J. Mach. Learn. Res. **1**, 211–244 (2001).

[19]D. P. Wipf and B. Rao, “An empirical bayesian strategy for solving the simultaneous sparse approximation problem”, IEEE Trans. Signal Process. **55**, 3704–3716 (2007).

[20]P. Gerstoft, C. Mecklenbrauker, A. Xenaki, and S. Nannuru, “Multi-snapshot sparse bayesian learning for doa”, IEEE Signal Process. Letters **23**, 1469–1473 (2016).

[21]Z. Zhang and B. Rao, “Sparse signal recovery with temporally correlated source vectors using sparse bayesian learning”, IEEE J. Sel. Topics Signal Process. **5**, 912–926 (2011).

[22]G. Ping, E. Fernandez-Grande, P. Gerstoft, and Z. Chu, “Three-dimensional source localization using sparse bayesian learning on a spherical microphone array”, J. Acoust. Soc. Am. **147**, 3895–3904 (2020).

[23]Z. Yang, L. Xie, and C. Zhang, "Off-grid direction of arrival estimation using sparse bayesian inference", IEEE Trans. Signal Process. **61**, 38–43 (2013).

[24]A. Xenaki and P. Gerstoft, "Grid-free compressive beamforming", J. Acoust. Soc. Am. **137**, 1923–1935 (2015).

[25]Y. Chi and Y. Chen, "Compressive two-dimensional harmonic retrieval via atomic norm minimization", IEEE Trans. Signal Process. **63**, 1030–1042 (2014).

[26]Y. Yang, Z. Chu, Z. Xu, and G. Ping, "Two-dimensional grid-free compressive beamforming", J. Acoust. Soc. Am. **142**, 618–629 (2017).

[27]Z. Zhang and B. D. Rao, "Extension of sbl algorithms for the recovery of block sparse signals with intra-block correlation", IEEE Trans. Signal Process. **61**, 2009–2015 (2013).

Chapter 5

Summary

For localizing the acoustic source, compressive sensing (CS) techniques have been applied to wide applications. The CS-based localization methods have been shown a high resolution capability and robustness against measurement noise. However, conventional CS-based localization methods suffer from computational instability and basis mismatch error. In this dissertation, 2 novel methodologies are presented in order to overcome the limitations of conventional CS technique.

Contributions of this dissertation are as follows :

- We introduced a CS-based method for localizing the three-dimensional acoustic source and developed the processing which deals with multiple frequency components jointly(methodology 1). The developed model enhances the localization accuracy and the reconstruction stability compared to conventional CS-based model by promoting the spectrally joint sparsity.
- We firstly developed an off grid method applicable to the three-dimensional localization problem(methodology 2). By reducing the basis mismatch error, we could obtain the accurate localization results and reduce the computational burden. The simulated and experimental results demonstrated advantages of the

proposed method, including capability to prevent the basis mismatch.

- We studied tip vortex cavitation phenomenon exploiting the localization results. We verify that estimated source locations are physically meaningful and matched for visual observation results.

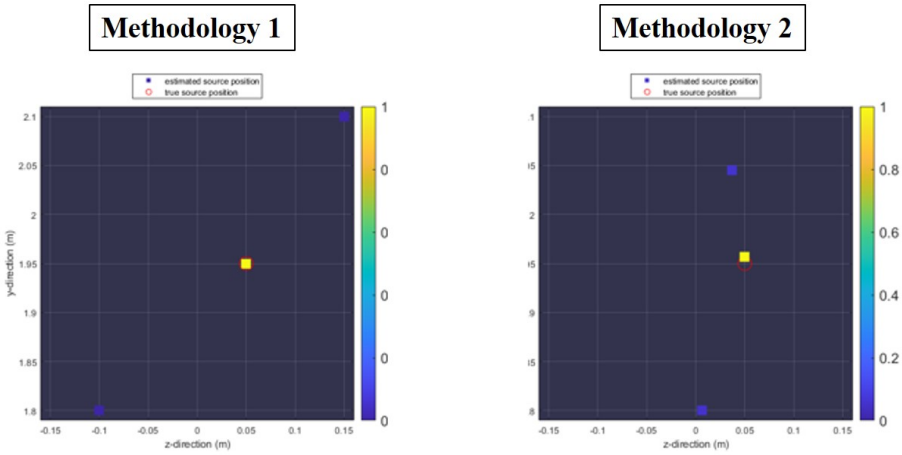

Figure 5.1: Comparison of the localization results : no basis mismatch is present, SNR=10dB

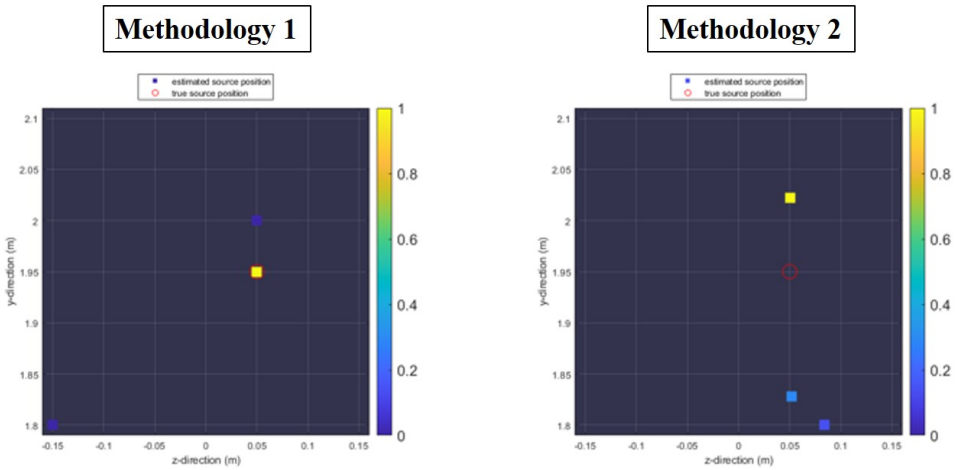

Figure 5.2: Comparison of the localization results : no basis mismatch is present, SNR=0dB

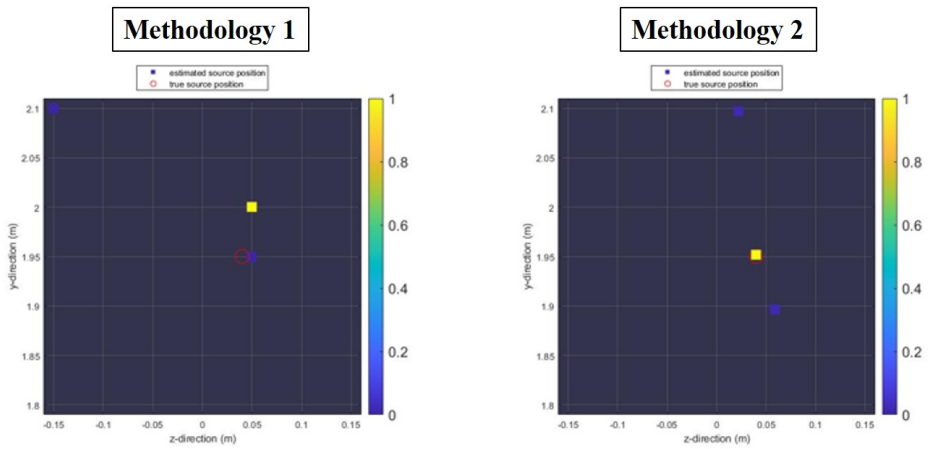

Figure 5.3: Comparison of the localization results : basis mismatch is present(basis mismatch = 0.01m, grid span = 0.05m), SNR=10dB

초 록

압축센싱 기반 접근법을 이용한 수중음향 소음원의 위치 추정 기법 연구

박민석
조선해양공학과
서울대학교 대학원

삼차원 음향 소음원의 위치추정은 잠수체, 산란체, 캐비테이션 소음원의 분석을 위해 필수적인 과정이다. 전통적인 빔형성 기법은 강인한 위치 추정 결과를 제공하나, 하나의 소음원의 위치만을 구분할 수 있는 저해상도의 결과를 보인다. 고해상도의 위치 추정 결과를 얻기 위해 최근 압축센싱 기반의 위치 추정 기법들이 사용되어 지고 있다. 압축센싱 기법은 희소성을 가진 신호의 획득,처리,복원에 효과적인 방법이며 영상처리, 수중음향, 최적화 문제 등에서 널리 활용되어지고 있다. 수중 소음원의 위치 추정을 위하여 압축센싱 기밥의 기법들이 적용되어 왔으며 전통적인 빔형성 기법에 비하여 해상도 측면에서 더 나은 성능을 보여주었다.

하지만 이러한 해상도 측면의 성능 향상에도 불구하고 압축센싱 기반의 방법은 여전히 문제점들을 가지고 있다. 첫번째, 압축센싱 기법은 전통적인 빔형성 기법에 비해 수치 연산 과정이 불안전성을 가진다. 비록 고해상도의 성능을 보여주나 압축센싱 기법은 수치해석 과정에서 불안정한 모습을 보여주며, 안정적인 복원을 저해한다. 두번째, 기저불일치로 인한 오차가 정확한 소음원의 위치 추정을 저해한다. 게다가 3차원 소음원의 위치 추정 문제는 이러한 기저 불일치를 해결할 수 있는 기법이 아직까지 개발되지 못하였다.

본 논문은 기존의 압축센싱 기반의 위치 추정 기법이 가지는 문제점을 파악하고 3차원 위치 추정 문제를 다룰 수 있는 향상된 압축센싱 기법을 소개한다. 탐색 공간 사이의 높은 상관관계로 인하여 발생하는 해의 불안정성을 해결아기 위하여 “다중 주파수 상관 처리기법”을 소개하고, 3차원 위치 추정문제에서 기저불일치 문제를 해결할 수 있는 “유동 탐색 격자 기법”을 소개한다. 제안된 기법은 전통적인 빔형성 기법에 비하여 정확한 위치 추정 결과를 제공하며 실험 데이터를 통한 위치 추정결과를 이용하여 이러한 주장을 뒷받침하였다. 본 연구에서는 수중음향 소음원의 3차원 위치 추정 문제를 중점적으로 다루었으나, 제안된 기법은 소나 및 레이더, 음향 소음원 위치 추정 문제에도 효과적으로 적용될 수 있을 것으로 기대된다.

주요어: 압축센싱, 빔형성, 캐비테이션, 위치추정, 블록 희소성, 베이지안 학습
학 번: 2015-21164